

# Spontaneous Emission Rate Enhancement Using Optical Antennas

*Nikhil Kumar*



Electrical Engineering and Computer Sciences  
University of California at Berkeley

Technical Report No. UCB/EECS-2013-107

<http://www.eecs.berkeley.edu/Pubs/TechRpts/2013/EECS-2013-107.html>

May 17, 2013

Copyright © 2013, by the author(s).  
All rights reserved.

Permission to make digital or hard copies of all or part of this work for personal or classroom use is granted without fee provided that copies are not made or distributed for profit or commercial advantage and that copies bear this notice and the full citation on the first page. To copy otherwise, to republish, to post on servers or to redistribute to lists, requires prior specific permission.

### Acknowledgement

First, I'd like to thank my advisor, Professor Eli Yablonovitch for his mentorship and guidance over the past several years. His support, arguments and criticisms have been crucial to my growth as a graduate student and individual. I'd also like to thank Professor Ming Wu and Professor Xiang Zhang for their review of this dissertation.

I'd like to thank all my lab mates at Berkeley for their great insights and helpful discussions. I'd especially like to thank Michael Eggleston and Kevin Messer who were a big part of the work in this dissertation.

And to all those who helped me get through graduate school in the lab and outside, especially Matteo Stafforoni and Sapan Agarwal.

And of course my loving parents. If it weren't for them, I wouldn't have been born.

**Spontaneous Emission Rate Enhancement Using Optical Antennas**

By

Nikhil Kumar

A dissertation submitted in partial satisfaction of the  
requirements for the degree of

Doctor of Philosophy

in

Engineering – Electrical Engineering and Computer Sciences

in the

Graduate Division

of the

University of California, Berkeley

Committee in charge:

Professor Eli Yablonivitch  
Professor Ming C. Wu  
Professor Xiang Zhang

Spring 2013



## Abstract

### Spontaneous Emission Rate Enhancement Using Optical Antennas

by

Nikhil Kumar

Doctor of Philosophy in Engineering - Electrical Engineering and Computer Sciences University of California, Berkeley

Professor Eli Yablonovitch, Chair

The miniaturization of electronics has relentlessly followed Moore's law for the past several decades, allowing greater computational power and interconnectivity than ever before. However, limitations on power consumption on chip have put practical limits on speed. This dissertation describes the role that optical antennas can play in reducing power consumption and increasing efficiency and speed for on-chip optical interconnects.

High speed optical communication has been dependent on the laser for its narrow linewidth and high modulation bandwidth. It has long outperformed the LED for both practical reasons and its suitable physical characteristics. Lasers however have some downsides when considering short distance communications which may not require narrow linewidths. Typically, they require high powers, take up more space and the rate is inherently limited by gain saturation. LEDs on the other hand are limited by spontaneous emission, a rate that is dependent upon its electromagnetic environment. The use of metallic optical nano-antennas can significantly increase a light emitters coupling to its environment and potentially achieve a rate orders of magnitude faster than stimulated emission. Coupling a light emitter into an efficient nano-optical antenna serves three purposes – 1) a much faster modulation speed can be achieved due to a faster rate of spontaneous emission, 2) the footprint of such a device would be shrunk to the nano-scale, ultimately necessary for large scale integration and 3) the overall efficiency of the emitter can be increased.

While the main motivation behind this work is for short distance communications, optical antennas can serve in a host of applications including photodetectors, solar cells, nano-imaging, bio-sensing and data storage.

In this thesis we derive the theory behind optical antennas and experimentally show an enhanced spontaneous emission rate of  $\sim 12.5x$  for bar antennas and  $\sim 30x$  for bowtie antennas.

# Acknowledgements

First, I'd like to thank my advisor, Professor Eli Yablonovitch for his mentorship and guidance over the past several years. His support, arguments and criticisms have been crucial to my growth as a graduate student and individual. I'd also like to thank Professor Ming Wu and Professor Xiang Zhang for their review of this dissertation and serving on my qualifying exam committee.

I'd like to thank all my lab mates at Berkeley for their great insights and helpful discussions. I'd especially like to thank Michael Eggleston and Kevin Messer who were a big part of the work in this dissertation.

And to all those who helped me get through graduate school in the lab and outside, especially Matteo Stafforoni and Sapan Agarwal.

And of course my loving parents. If it weren't for them, I wouldn't have been born.

# Table of Contents

1	Introduction.....	1
1.1	Motivations.....	1
1.2	Limitations of Electrical Interconnects.....	2
1.3	Advantages and Challenges of Optical Interconnects.....	3
1.4	Introduction to Optical Antennas.....	5
1.4.1	Photodetectors and Solar Cells.....	6
1.4.2	Nanoimaging.....	6
1.4.3	Bio-sensing.....	7
1.4.4	Data Storage.....	7
1.5	LEDs vs Lasers.....	9
2	Antenna Review and Spontaneous Hyperemission.....	11
2.1	Antenna History.....	11
2.2	Antenna Design Concepts.....	12
2.2.1	Larmour Formula for a Dipole.....	12
2.2.2	Q of an electrically small Antenna.....	15
2.2.3	Circuit Model and Maximum Power Transfer.....	16
2.2.4	Capture Cross-section and Directivity.....	19
2.3	Metal Optics.....	21
2.3.1	The origin of Kinetic Inductance.....	21
2.3.2	Drude Model.....	22
2.4	Spontaneous Emission Rate Enhancement.....	25
2.4.1	Quantum Mechanical Description of Spontaneous Emission.....	25
2.4.2	The Purcell Effect.....	27
2.4.3	Optical Antenna Assisted Spontaneous Hyper Emission.....	30
2.4.4	Equivalence of Purcell and Antenna Enhancement.....	32
2.4.5	Modulation Speed.....	35
2.4.6	Spontaneous Hyper Emission from a semiconductor.....	36
3	Design and Fabrication.....	37
3.1	Bar Antenna Fabrication.....	38
3.2	Bowtie Antenna and Dipole Antennas.....	40
4	Experimental Results and Discussion.....	42
4.1	Light Trapping and Extraction Enhancement.....	43
4.2	Resonant Pump Enhancement.....	45
4.3	Bar Antenna Results.....	46
4.4	Bowtie Antenna Results.....	49
5	Future Work and Conclusions.....	54
	Bibliography.....	56
	Appendix 1: Derivation of Fields from a Hertzian Dipole.....	60
	Appendix 2: Methods for Deriving Spontaneous Emission.....	62

# Chapter 1: Introduction

This thesis describes our efforts to engineer and increase the rate of spontaneous emission using optical antennas while concurrently improving quantum efficiency. We will show theoretically and experimentally that semiconductors coupled to antennas can efficiently radiate at a faster rate and that they can potentially eclipse lasers in speed while drawing less power. The main motivation behind the project is ultrafast and efficient optical communications for intra-chip and inter-chip interconnects. However, other applications for optical antennas exist and the design rules and physics can potentially be applied to a variety of photonics applications including Surface Enhanced Raman Scattering, fast photo-detectors and solar cells.

This dissertation is organized in the following way:

Chapter 1 discusses the motivation of optical antennas and spontaneous hyper emission and its potential role in interconnects. It then details necessary concurrent technologies to make it viable, as well as competing technologies in this space.

Chapter 2 discusses the theory, designs and figures of merit for semiconductor optical antennas.

Chapter 3 is devoted to the fabrication challenges and experimental setup used to characterize the devices

Chapter 4 details the experimental characterization and analysis of the devices

Chapter 5 proposes future work on semiconductor optical antennas

## 1.1 Motivation

In the last several years energy considerations have quickly placed a limit on speed in microprocessors (Fig 1.1). Chief in power consumption is electrical interconnects, detailed in the 2007 ITRS report – "...at 0.13 $\mu$ m approximately 51% of microprocessor power was consumed by interconnects... without changes in design philosophy, in the next five years up to 80%"[1]. Moore's law dictates why a growing percentage of power consumption is in interconnects. While capacitances for devices shrink with each node, the capacitance of interconnects are stuck at 1-3pF/cm. This is because the capacitance of a wire depends only logarithmically on the ratio conductor spacing, so  $C \sim \epsilon_r$ , and thus  $CV^2 \sim 1$ pJ/bit for a 5mm wire. Optical interconnects present a very attractive option as long as the system power budget comes in at less than 1pJ/bit due to further limitations in electrical interconnects.

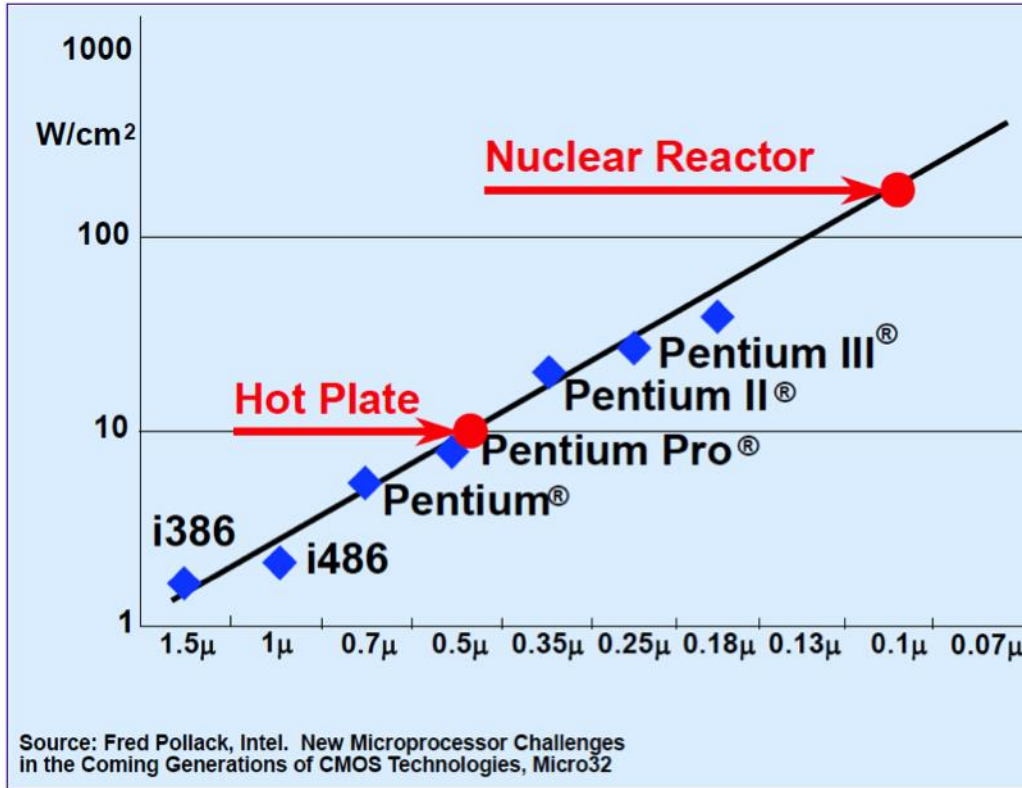


Fig 1.1 Power consumption as a function of process node [2]

## 1.2 Limitations of Electrical Interconnects

Electrical interconnects have been incredibly successful in routing complex signals at low cost, and has enabled a boom in information processing in the last several decades. However, moving towards faster and more power efficient electronics there lie a few limitations.

Firstly, amongst the three core energy consumers on chip; logic operations, memory and interconnects, electrical interconnects are most power hungry due to the need to charge and discharge wires. Secondly, compared to optics, metal wires suffer from signal attenuation due to resistance and dielectric loss, effecting higher frequencies worse and distorting signals. One solution is to make the cross sectional area larger to reduce the resistance; however, this imposes a limit on the density of the wiring as interconnects quickly can take up all available space. For long wires this also increases cost. On the other hand, scaling down the wires in all 3 dimensions does not improve the RC time constant and thus the bitrate stays the same as seen below where  $\rho$  is the resistivity,  $L$  is the length and  $A$  is the cross sectional area.

$$(1.1) R = \frac{\rho L}{A}$$

$$(1.2) C \sim \epsilon L$$

The capacitance  $C$  depends only logarithmically on the ratio of wire size to separation and thus the bandwidth can be written as in eq. (1.3) where  $B_0$  is a constant equal to  $\sim 10^{16}$  for RC limited lines on chip and  $\sim 10^{17}$  for off-chip lines[3].

$$(1.3) B \leq B_0 \frac{L^2}{A}$$

Thus the bandwidth of the system is limited when wiring takes up all the available space and the energy of the system is determined by the charging and discharging of these wires.

The limitations of electrical wires have been known since the early 1980's and in present days even with sophisticated techniques electronic systems already experience these limits prompting the shift to the lower resistance copper and the line to be split up into segments. This does increase the bandwidth but significantly increases delay caused by repeater circuits. Furthermore it does not overcome the fundamental limitations imposed by electrical interconnects. For that, optics is considered a viable approach to bypass these limitations.

### **1.3 Advantages and challenges for Optical Interconnects**

Fiber optic cables are of course already widespread in long distance communications and are increasingly being adopted in data centers due to the sheer amount of information that can be compressed and relayed on a single fiber. A single mode fiber can carry tens of terabits per second in principle, while other factors such as the availability of high speed transmitters, receivers and repeaters, as well as material effects such as dispersion and non-linear processes put a practical limit on the available bandwidth.

Free space communications don't suffer from dispersion or non-linear processes that take place in a fiber medium; however in the optical regime it requires line of sight due to absorption and reflection from materials. While seemingly a more "radical" option, this may be path forward in the future for high-speed board-to-board communications. Free space components such as micro-lenses, MEMs mirrors and liquid crystals, which debuted as consumer products for the flat screen televisions have found a viable market in telecom. System vendors such as Finisar and JDSU use these as commercial technologies in wavelength-selective switches, a key component in reconfigurable add drop multiplexers [4].

Far more useful is waveguided optics and these companies are increasingly becoming more interested in planar lightwave circuits or PLCs which has promise in cutting costs from packaging and the bill of materials by integrating all components onto one mass producible chip. Additionally, these technologies can be smaller and faster and require fewer discrete components such as splitters, polarization rotators and lenses, which obviate the need for hermetic sealing. The promise of integration also introduces a new set of functions that would be difficult or costly to implement traditionally, such as the ability to reroute traffic without dropping any information.

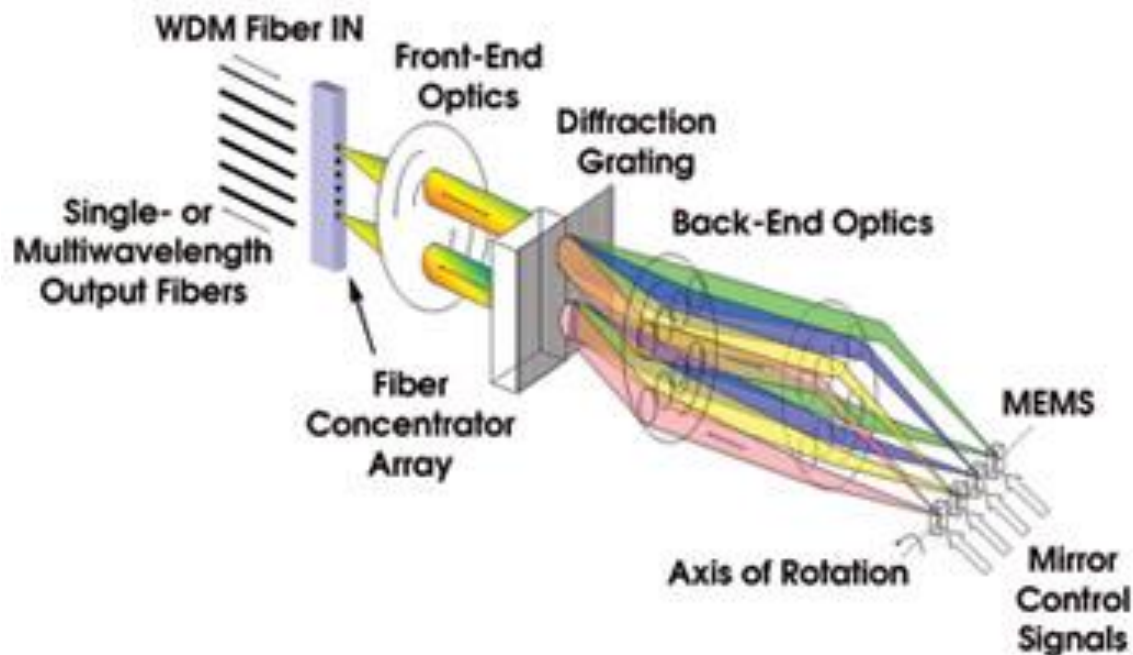


Fig 1.2 Schematic of a wavelength selective switch controlled by MEMS mirrors. [5]

Most recently, there has been a strong push towards silicon photonics – integrating photonics onto a silicon platform. Leveraging decades of silicon processing in CMOS foundries for computer chips, silicon is cheap, scalable and is readily developed. Silicon has the added benefit of transparency at infrared wavelengths – allowing it to be used as a waveguide medium and with germanium growth now becoming a widespread foundry process – detectors can be made at these wavelengths. Side by side, CMOS electronics integrated with a silicon photonic layer appears to be a viable future technology. Industry players include Luxtera, IBM, Intel, Kotura (recently acquired by Mellanox) and in the past 5 years Aurrion and Skorpios. Luxtera, which uses an external laser, couples light into its silicon platform and has achieved a 4x28Gbps transceiver targeted towards the datacom market. More recently start-up lightwire was purchased by Cisco for its low-cost, small form factor and power efficient silicon-based modulator which is now offered as a product. Even more promising is the ability to integrate III-V material onto silicon using a variety of bonding techniques including direct semiconductor bonding, metal to metal bonding and adhesives. Currently, Skorpios and Aurrion hope to achieve complete integration using CMOS compatible processes and thus far both have demonstrated lasers directly integrated onto silicon.

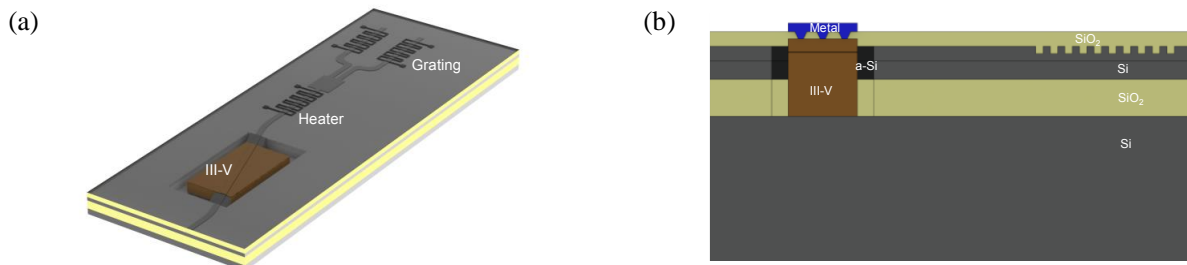


Fig. 1. (a) Illustration of the integrated tunable CMOS laser. (b) Cross-section view of the geometry.

Fig 1.3 Skorprios' integrated tunable CMOS-compatible laser with an external cavity [6]

With the limitations of electrical interconnects discussed earlier, it is not a far leap to imagine integrating light emitters for ultrafast and power efficient on chip or chip-to-chip communications. Moreover, as just described companies are already attempting the same for the telecom and datacom markets proving the validity of this research path. The light could be created, modulated and detected on chip without ever requiring active alignment or coupling to an external source. One solution to making an ultrafast, efficient emitters stems from optical antennas.

## 1.4 Introduction to Optical Antennas

Antennas are well established in many areas of modern technology from consumer based electronics, such as wireless routing and cell phones, to the high end business and defense markets such as satellites and radar. Traditionally these applications have been in the microwave/RF regime and techniques for their optimizations and have been heavily studied and are well known. But despite their widespread use and firm theoretical foundation, until recently designing and fabricating antennas in the optical regime has not been possible. This is primarily due to the small length scales required for an optical antenna, since the characteristic length of an antenna is on the order of a half-wavelength in the medium. In the last decades these nanoscale structures have become accessible with tools such as electron beam lithography and even optical lithography in top-down fabrication approaches.

The primary function of an optical antenna is the same as its traditional microwave counterpart – to convert localized energy, stored in electromagnetic currents, to the free-space radiation field in the case of transmission, or vice versa in the case of a receiving antenna. This allows the focusing of light to hotspots that are much beyond the diffraction limit. There are a host of applications for a well designed optical antenna. A few will described here while the main application – for ultrafast, low power and efficient nanoLEDs and the main research – spontaneous hyper emission will be described in the rest of this work.

### 1.4.1 Photodetectors and Solar Cells

Traditionally the area of a photodetector is bounded by the diffraction limited optics that focus light upon it. Consequently the noise associated with the detector has a lower limit as the dark current scales with area and the shot noise associated with this, scales as the square root of the area. As will be seen in chapter 2, an antenna has the ability of capturing light outside its physical dimensions and focusing it to a small spot thus reducing the required area of the absorbing material. This factor can be 100x or more and since the signal remains the same, the antenna boosts the signal to noise ratio of the detector by 10x. Additionally the thickness of the absorbing layer can be reduced as the antenna focuses the light in the 3<sup>rd</sup> dimension as well. This factor in thickness plays an important role in the speed of the device, since this depends on the time it takes carriers to be swept through the device.

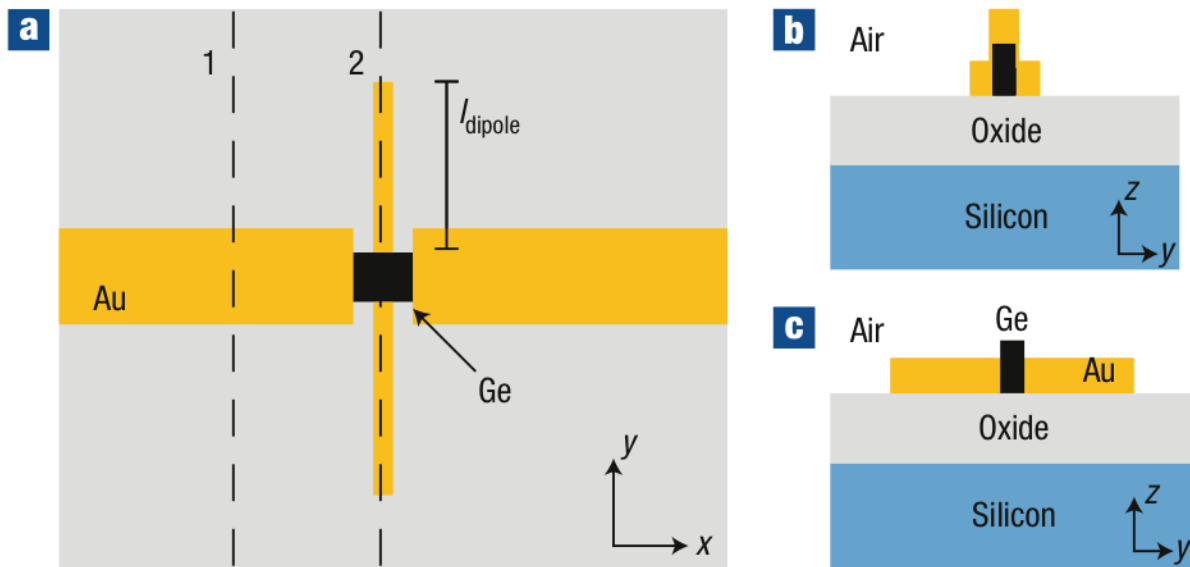


Fig1.4. From [7], a) a schematic view of an antenna fabricated on Ge b) cross section through 1. c) cross section through 2

It is a little less obvious if there is a benefit to solar cells from optical antennas. It can reduce the thickness required of the absorbing layer, but antennas are resonant structures, which inherently have a finite bandwidth as opposed to the wide bandwidth that is optimal for solar cells. In the optical regime, antennas also suffer from loss, which can erase any gains from the antenna itself. Nevertheless, researchers are working on it to improve efficiencies and reduce thicknesses [8].

### 1.4.2 Nano-imaging

The analogy between optical probes and antennas came after near-field optical microscopy had become a mature technology and tip-enhanced fluorescence from NSOMs had been observed

[9]. However, the concepts can be readily applied and understood and 10-50nm features can be resolved. The first of these experiments involved scanning a spherical gold particle to a probes close to fluorescent molecules enhancing the fluorescence and reducing lifetimes [10][11][12].

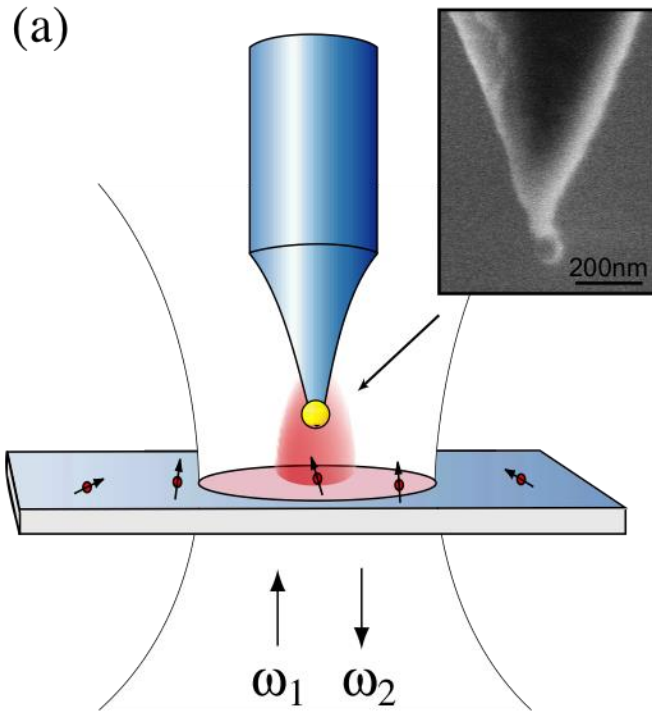


Fig 1.4. From [12]. An schematic and SEM image of a nanoparticle of gold upon an optical probe

### 1.4.3 Bio-sensing

Although the previously described experiments do support bio sensing, ideally there would be platform upon which aqueous molecules can be detected, which would replace mass spectroscopy as the choice of molecular detection. To this end researchers have focused their efforts on engineering Surface Enhanced Raman Scattering (SERS) by fabricating antennas with gaps in them such that dilute molecules could easily be sensed. Antennas seem ideally suited for SERS as the molecules experience an enhancement in the pump intensity as well as an enhancement in the emission since typically most antennas have a bandwidth that covers both peaks [13] [14].

### 1.4.4 Data storage

Perhaps closest to commercial production is the use of optical antennas in heat-assisted magnetic recording (HAMR). Much like Moore's law, in order to scale hard-drive capacity the density of

bits stored per unit area. Simply decreasing the grain size of the magnetic medium increases its instability to random thermal fluctuations. To overcome this the magnetocrystalline anisotropy energy must be increased, the downside being a required increase in magnetic field from the write head.

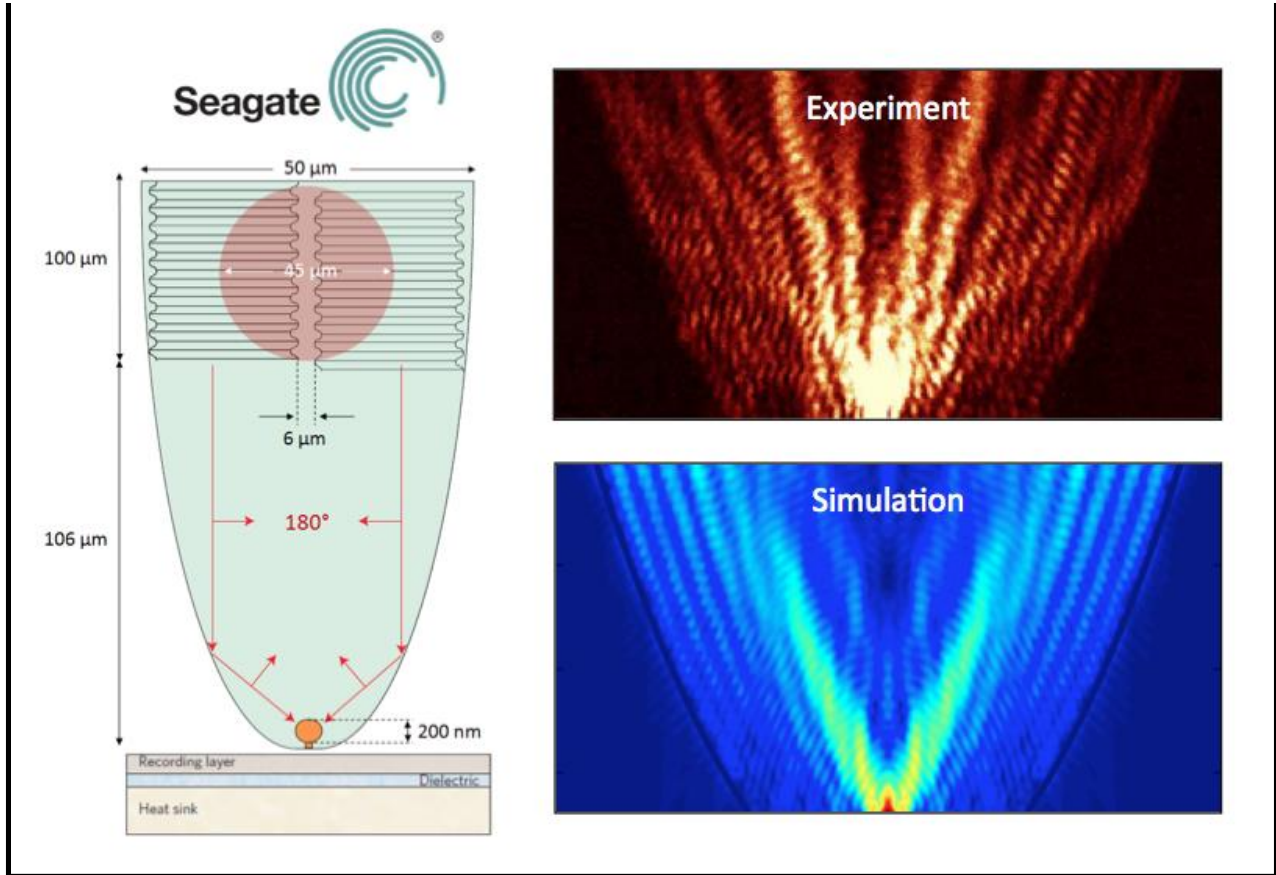


Fig 1.5. In this Seagate configuration, a laser is focused upon a grating which is adiabatically tapered to a lollipop antenna. The antenna provides the local heating required to flip the magnetic bit [15].

The write heads cannot achieve such high fields due to material limits. Fortunately, the anisotropy is heavily temperature dependent, and thus local heating the grain allows the bit to be flipped. The grain sizes in question are  $\sim 30\text{nm}$  and thus due to the diffraction limit laser heating is not an option. Near-field devices such as optical antennas on the other hand can provide an electromagnetic and consequently a thermal hotspot on the nanoscale and therefore are the leading candidates for this technology.

## 1.5 LEDES vs Lasers

Both LEDs and Lasers are dependent on a semiconductors ability to radiate light. This ability stems from the materials intrinsic dipole matrix element, a factor that determines the interaction between light and matter. Completely analogous to a classical radiating dipole and described in chapter 2, this dipole length is short in materials  $<1\text{nm}$  compared to its emission wavelength and thus most semiconductors, atoms and molecules are weak and slow.

Lasers make up for this by relying upon stimulated emission, which depends on high intensities of light being trapped in the material, instigating stimulated emission. The stimulated emission rate still depends upon the intrinsic dipole, which is fixed, but also upon the density of photons in the material. This allows for high powers, as this rate can be fast and for practical reasons, the laser has long outperformed the LED. However, the modulation speed of lasers is inherently limited by the rate of stimulated emission in the device and typical devices reach speeds in the 10's of Ghz due to gain saturation. Additionally lasers are power hungry. First, in order to get significant amounts of stimulated emission, it must be biased above its threshold which requires a significant amount of current. And second, the modulation bandwidth is proportional to the square root of the energy density, requiring greater pumping to achieve higher bandwidths.

LEDs on the other hand rely upon spontaneous emission. Unlike lasers, its rate is not dependent upon incident light and as mention previously its rate, has been slow  $\sim 1\text{ns}$  leading to a 100Mhz modulated LEDs. However it is depend on its electromagnetic environment i.e. the density of optical states. Described by Purcell in 1948, imagining an emitter trapped in a cavity one can deduce the spontaneous emission increases by  $\sim Q/V$  where  $Q$  is the quality factor of the cavity and  $V$  is the effective volume. The use of metallic optical nano-antennas can confine these modes into volumes much smaller than the diffraction limit of light with moderate  $Q$ s. This can potentially yield orders of magnitude in enhancement but until recently, engineering this optical density of states has not been explored due to limitations in fabrication. The enhancement works two fold, 1) the rate of emission is increased leading to higher modulation bandwidths and 2) the radiative rate is increased compared to non-radiative recombination and the efficiency is increased. Thus the oft forgotten LED has the potentially to outperform lasers in speed, efficiency and size.

One key distinction between Lasers and LEDs is the linewidth of the emission. The success of long-haul optical communication has been dependent on this, as it allows dense wavelength division multiplexing (DWDM) with minimal cross-talk and dispersion in the optical fiber. The current ITU grid in the c-band (the wavelengths surrounding 1550nm) limits the spacing between wavelengths to 50Ghz and this is expected to decrease to 25Ghz and even further as bandwidth becomes more in demand. Additionally lasers emit light that is coherent allowing balanced detectors which significantly improve the signal to noise ratio.

A nanoLEDs cannot compete with either of these and so is not suitable for high-speed transmission along a fiber for long distance communications. The linewidth of a nanoLED is reduced due to less of a build up in carrier concentrations for a given injection current; however is still too broad to be used in WDM systems. Where they do have a niche, is for efficient, high

speed on-board or-on chip optical communications where distances are short and dispersion may not be as big of an issue.

# Chapter 2: Antenna Theory and Spontaneous Hyper Emission

## 2.1 Antenna history

The first demonstrated wireless electromagnetic system dates back to 1886 in which Heinrich Hertz successfully transmitted and received electromagnetic radiation with antennas. He produced a spark in the gap of a 4m long  $\lambda/2$  dipole which was sensed by a nearby loop antenna creating spark in the gap of a loop. Fueled by the first success of spark gap antennas, much work went on in the late 1800's but it was not until 1901 Marconi demonstrated the first transatlantic transmission of the letter 'S' in Morse code from England to Newfoundland, a distance of 2,200 miles [16]. The transmitting antenna was set up with 50 vertical wires acting at a wavelength at what is believed to be ~350m and the receiving antenna was a ~200m wire pulled by a kite. Although crude and facing much skepticism, he later went on to build more convincing systems and prove that wireless communication could span 100s of kilometers, ultimately winning the Nobel prize in physics in 1909 for his contributions in radio [17].

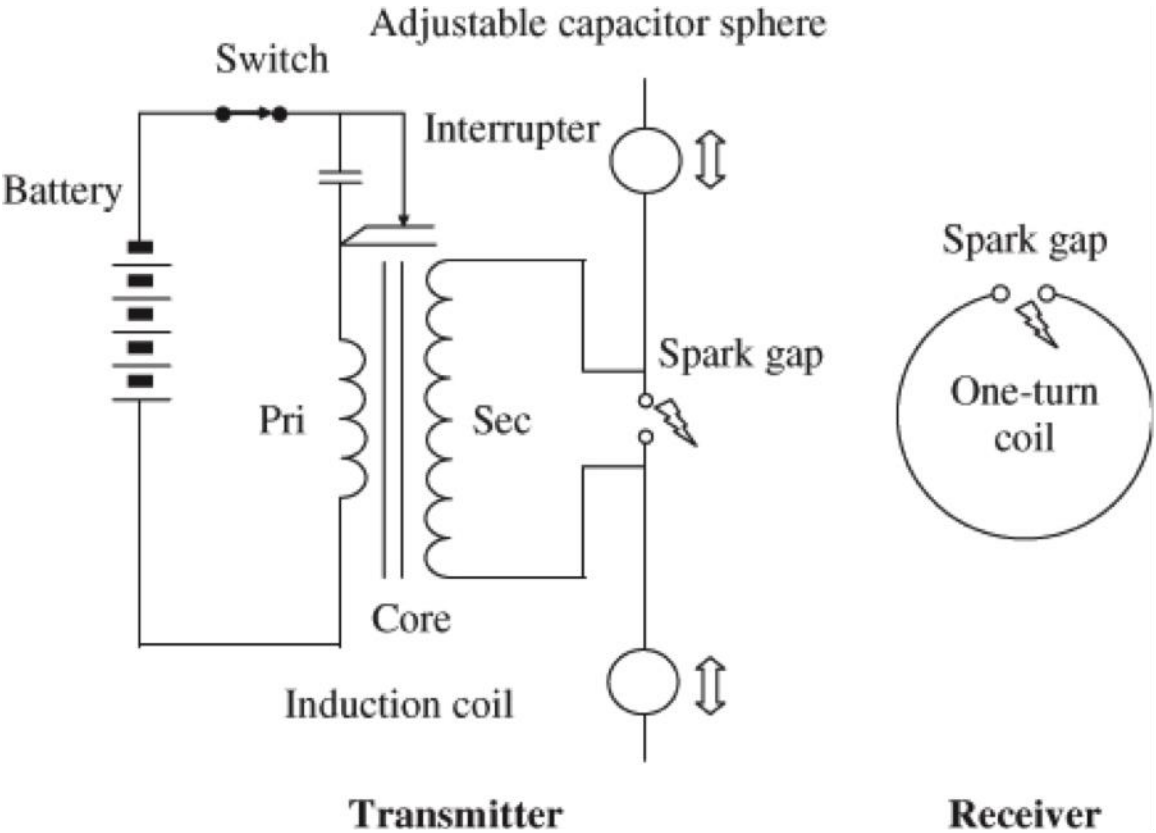


Fig 2.1 A schematic of the first demonstrated transmitter and receiver developed by Hertz.

Until the 1940s antennas resembled the wires and frequencies (up to UHF) that Marconi used. Only the technological advances spurred by the crisis of World War II really launched antenna technology into the modern age. The advent of the magnetron allowed high powered 1GHz signals and above to be produced and new elements such as waveguide apertures, horns, phased arrays, reflectors and new radar designs were introduced [18][19]. So crucial were these advances during that war, that it could be claimed that the historic battle of Britain was won based almost entirely upon the allies more advanced radar systems.

In the 1960's through 1980's advances in computer technology made it possible to use numerical methods such as Finite-Difference, Finite Element, the method of moments and the geometrical theories of diffraction to solve complex electromagnetic antenna problems. While they cannot replace intuition and the knowledge gained during the World War II era, they play a significant role in today's design of antenna systems and can predict operation to a great deal of accuracy obviating the need for intermediate testing in some cases [18].

In the 1970's the microstrip and patch antenna were introduced, an extremely useful design that is typically is printed on circuit boards for the UHF band(300Mhz to 3Ghz). Its simple, lightweight, inexpensive, and rugged design have superseded its disadvantages which are lower efficiency and narrow bandwidth [18]. They are commonly found in GPS systems, RFIDs, airplanes, missiles and satellites.

As described in chapter 1, recently antenna design has been reintroduced to optical frequencies as nano-scale processing has now made antennas at these dimensions attainable. The rest of chapter 2 will describe fundamentals of antenna theory, semiconductors and enhanced spontaneous emission rate.

## 2.2 Antenna Theory and Design Concepts

### 2.2.1 Larmour formula for a dipole

An antennas characteristic to radiate comes simply from the fact that an accelerating charge radiates energy. The derivation was first given in 1887 by J.J Larmour who calculated the total power from an accelerating charge. Edward Purcell in 1960 found the solution to this problem using geometry and intuition, which will be reproduced here.

Consider a point charge moving at a speed  $v_0 \ll c$  that decelerates uniformly in time  $t_0$ . At time  $T \gg t_0$ , the distance this "information" or change in field has traveled is  $R = ct$ , represented by the inside of shaded region. Now the ratio of the transverse electrical field to the radial electrical field can be found through geometry:

$$\frac{E_T}{E_R} = \frac{v_0 T \sin\theta}{ct_0} = \frac{aR \sin\theta}{c^2}$$

where  $c$  is the speed of light,  $a$  is the magnitude of acceleration,  $E_T$  is the transverse electric field,  $E_R$  is the radial electric field and  $\theta$  is the angle of the particle to the point in question.

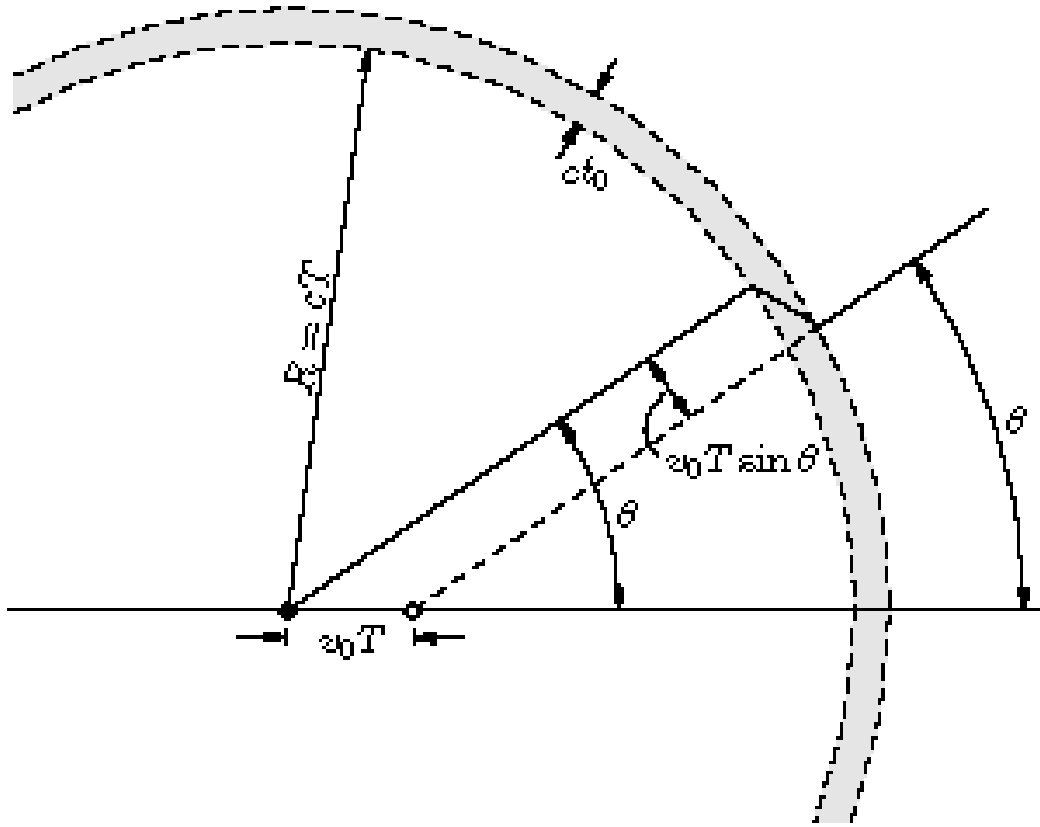


Fig 2.2 Geometry of the electric field lines emanating from a moving charge at time 0 and T [20]

Since  $E_R$  is given by coulomb's law,  $E_T$  is:

$$E_T = \left( \frac{aR \sin \theta}{c^2} \right) \left( \frac{q}{4\pi \epsilon_0 R^2} \right) = \frac{aq \sin \theta}{4\pi \epsilon_0 cR}$$

Notice that this field falls off as  $1/R$ . The power radiated will necessarily fall off as  $1/R^2$  since power is proportional to  $|E|^2$  and so the total energy within the shaded region will always remain constant. Now taking the pointing vector and integrating over all angles yields the larmour radiation formula

$$S = \epsilon_0 c |E|^2$$

$$P = \frac{q^2 a^2}{6\pi \epsilon_0 c^3} \quad (2.1)$$

Thus any accelerating charged particle radiates energy. Likewise, an oscillating dipole or the time varying currents in an antenna have electrons accelerating and decelerating, necessarily

emitting radiation. For the case of a time varying dipole, with  $qx = qx_o \cos(\omega t)$ , where  $x$  is the electron's position, The larmour formula accurately predicts the time-averaged power radiated as follows:

$$P = \frac{q^2(2x_o)^2 \omega^4}{12\pi \epsilon_o c^3} = \frac{\pi}{3} \sqrt{\frac{\mu_o}{\epsilon_o}} \left(\frac{2x_o}{\lambda}\right)^2 (q\omega)^2 \quad (2.2)$$

On the right side of Eq2.4, the terms are rearranged to provide some insight. The term  $\sqrt{\mu/\epsilon} = Z_o \sim 377\Omega$  is the impedance of free space, the ratio between the electric and magnetic fields. The term  $(x_o/\lambda)^2$  is a scaling factor based on the size of the dipole and its emission wavelength. Finally, the term  $(q\omega)$  represents the magnitude of the current due to the oscillating dipole. For the case of only one charge moving instead of a dipole, the current is  $(q\omega/2)$ . Note that this is the total amount of power emitted from the antenna. In general, the antenna will radiate more power in some directions compared to others and needs a full vector analysis to derive (see appendix 1). Intuitively though, in the case of a upright linear antenna (fig 2.3), looking down the  $z$ -axis we do not see an acceleration by the electron and thus the antenna radiates only in the  $x$  and  $y$  plane.

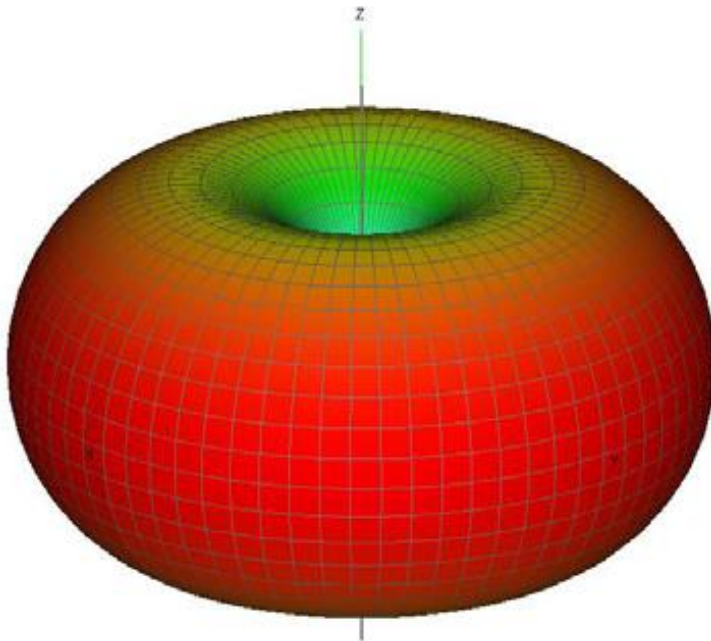


Fig 2.3. A constant E-field diagram of an oscillating dipole oriented along the  $z$  axis. Emission is preferentially radiated in the  $x$  and  $y$  directions.

Typically, in antenna problems the power is broken into its constituent parts as  $P=(1/2)I^2R_{rad}$  where  $I$  is the driving current and  $R_{rad}$  is the radiation resistance, a figure of merit signifying the amount of power emitted as radiation. In this case, we see that:

$$R_{rad} = \frac{2\pi}{3} Z_o \left( \frac{2x_o}{\lambda} \right)^2 \quad (2.3)$$

It is clear that small dipoles on the order of 1nm (such as molecules) are poor radiators at optical frequencies as their radiation resistances can be  $<0.01\Omega$ . Electrically driven short dipole antennas in the microwave region may have radiation resistances of  $1\Omega$ , also poor radiators. Longer antennas such as the  $\lambda/2$  dipole, require a more lengthy derivations as the current is not uniform along the length of the wire [18], but generally radiate much better. Here we will stress the importance of reciprocity in these device i.e. an antennas properties in transmission mode will be the same as that in receiving mode. This applies to radiation characteristics, bandwidth, matching networks and so forth. Typically an antenna will also have an imaginary component,  $X_{ant}$  that symbolizes either capacitance or inductance in the antenna.

### 2.2.2 Q of an electrically small Antenna

Another important figure of merit is the quality factor or Q of the antenna.

$$Q = 2\pi \frac{\text{energy stored}}{\text{energy lost per cycle}} = \frac{\omega}{\Delta\omega} \quad (2.4)$$

Good antennas will have  $Q=1$ , yielding a broadband operation. Certain structures, such as the infinite bowtie antenna or log periodic antennas are also known to have very broadband operation and are considered “infinitely broadband”. In general, smaller antennas will have higher quality factors, a phenomenon that has an effect on optical antennas, which by necessity are smaller than a half-wavelength. More on this will be described in a later section. Wheeler was the first to thoroughly investigate this phenomenon placing a limit on the lowest possible Q of small antennas [21], which was later verified by other works such as Lopez.

A short antenna, defined by wheeler as the length  $l < \lambda/(2\pi)$ , can be represented as a RC circuit since it is small compared to a wavelength and is in the quasi-static regime. In the case where it is purely capacitive, we can write Q as:

$$Q = \frac{1}{\omega RC} \quad (2.5)$$

The capacitance can be written as:

$$C = \epsilon_0 \frac{kA}{x_0} \quad (2.6)$$

where  $A$  is the area,  $x_0$  is the distance and  $k$  is a factor that includes fringing fields. The actual determination of  $A$  and  $d$  are not so important now as these will be lumped into an “effective volume”. Substituting  $R_{\text{rad}}$  from Eq 2.3 and  $C$  from Eq 2.6 into the formula for  $Q$  in Eq 2.5, and we get Eq 2.6. Notice that in this case  $x_0$  is both the plate separation as well as the total distance of the oscillating dipole.

$$Q = \frac{x_0}{\omega \frac{2\pi}{3} \sqrt{\frac{\mu_0}{\epsilon_0}} \left(\frac{x_0}{\lambda}\right)^2 \epsilon_0 kA}$$

$$Q = \frac{\lambda x_0}{\frac{4\pi^2}{3} c \sqrt{\frac{\mu_0}{\epsilon_0}} \left(\frac{x_0}{\lambda}\right)^2 \epsilon_0 kA}$$

$$Q = \frac{3\lambda^3}{4\pi^2 x_0 kA} = \frac{3}{4\pi^2} \frac{\lambda^3}{V_{\text{eff}}} \quad (2.10)$$

$V_{\text{eff}}$  is the effective volume of the antenna, which can vary depending on the field intensity outside the physical structure. The major point is that scaling down the volume of the antenna necessarily increases the  $Q$ . For optical antennas which are typically smaller than a half-wavelength

### 2.2.3 Circuit Model and Maximum power transfer

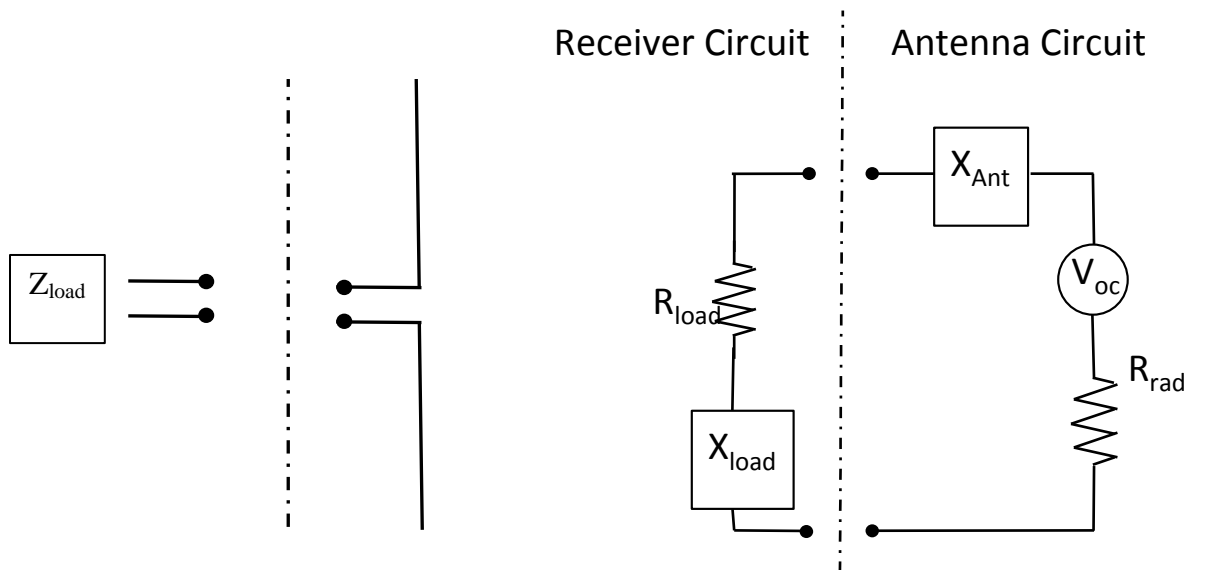


Fig 2.4 A receiving antenna circuit model

To simplify the characteristics of an antenna, a receiving or transmitting mode antenna can be structured as an equivalent circuit. In the case of receiving, the antenna is lumped as  $R_{rad}$  and  $X_{Ant}$ , while the load is represented as  $R_{load}$  and  $X_{load}$ .

The current flowing through the circuit is:

$$I_{Load} = \frac{V_{oc}}{(R_{rad} + R_{load}) + j(X_{Ant} + X_{load})}$$

And the time-average power transferred to the load is:

$$P_{load} = \frac{1}{2} I_{Load}^2 R_{load}$$

$$P_{load} = \frac{V_{oc}^2 R_{load}}{(R_{rad} + R_{load})^2 + (X_{Ant} + X_{load})^2}$$

Given a fixed  $R_{rad}$  which is what captures the power, we can calculate the value of  $R_{load}$  and  $X_{load}$  that will maximize  $P_{load}$  by differentiating with respect to  $R_{load}$  and equating to 0. Doing so gives us the conjugate matching conditions for maximum power transfer:

$$\begin{aligned} R_{load} &= R_{rad} \\ X_{load} &= -X_{Ant} \end{aligned} \tag{2.11}$$

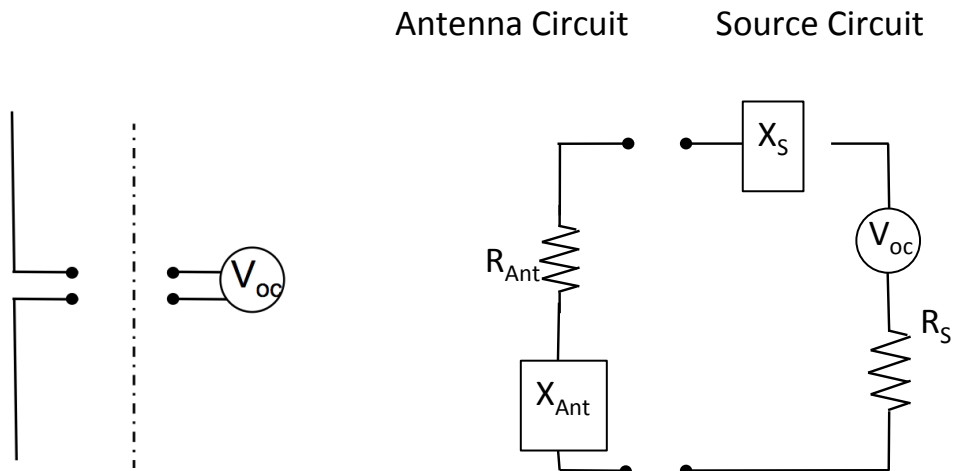


Fig 2.5 A transmitting antenna circuit

The same is true for a transmitting antenna with a *fixed* source impedance. In this case:

$$\begin{aligned} R_{source} &= R_{rad} \\ X_{source} &= -X_{Ant} \end{aligned}$$

It is important to note that this is true only for a fixed output impedance i.e.  $R_{rad}$  in the case of a receiving circuit and  $R_{source}$  for a transmitting circuit. This does not mean to achieve maximum power transfer to the source resistance should be increased to match  $R_{rad}$ . Also maximum power transfer does not equate to maximum efficiency as shown below. If  $\eta$  is the efficiency of the antenna it can be written as:

$$\eta = \frac{R_{rad}}{R_{rad} + R_{source}} \quad (2.12)$$

At maximum power transfer  $R_{rad}=R_{load}$ ,  $\eta=.5$  and the power is:

$$P_{load} = \frac{1}{2} \frac{V_{oc}^2 R_{load}}{(R_{rad} + R_{load})^2}$$

$$P_{load} = \frac{1}{8} \frac{V_{oc}^2}{R_{rad}}$$

Thus half of the power is transferred to the load and the other half is lost to  $R_{rad}$  in the form of scattering. The graph below exemplifies the trade off between power delivery and efficiency:

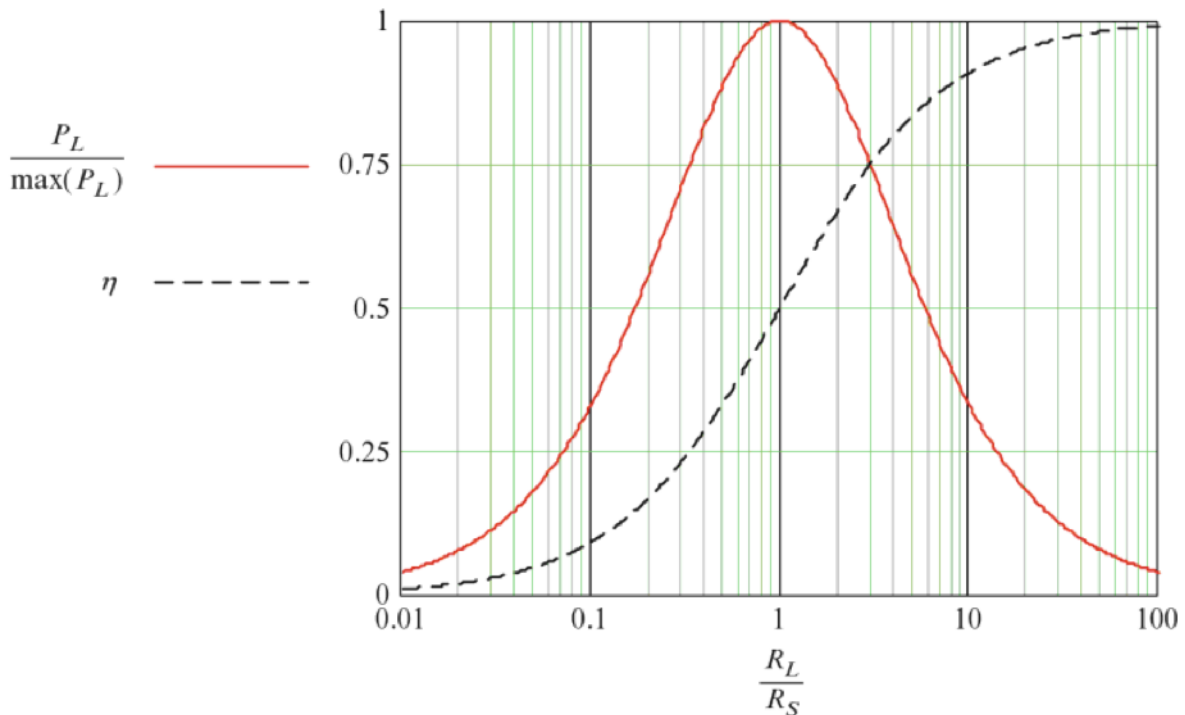


Fig 2.6 Plots of the efficiency and power transfer as a function of  $R_L/R_{Source}$  applicable to any circuit with a source and load[22]. Note the semilog scale.

The value of  $\eta$  increases as the ratio of  $R_{Load}/R_{Source}$  increases, however the source sees a larger resistance and the overall current in the circuit falls, decreasing the power transmitted to the load.

## 2.2.4 Capture Cross Section and Directivity

Another important parameter is the capture cross section of an antenna, that is the ratio between the power captured and the impinging light intensity. Interestingly, this ratio is more or less constant for a *matched* network, meaning the power captured is roughly independent of the size of the antenna. For small antennas we can see why this might be the case.

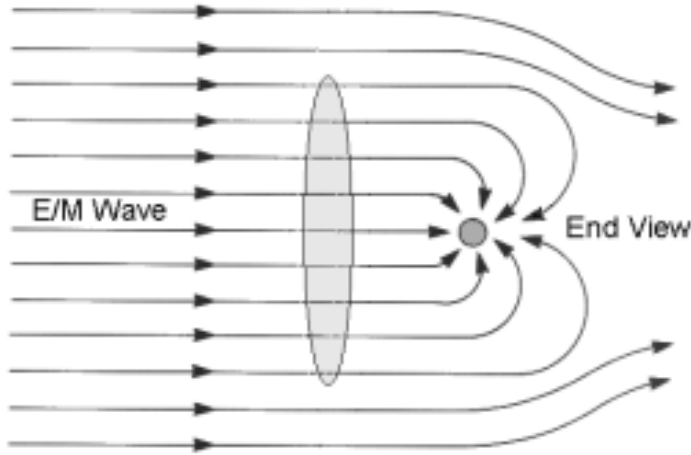


Fig 2.7 A schematic of Electric flux lines upon a metallic particle, illustrating that a small particle can capture a energy density reaching past its physical size.

$$A_{eff} = \frac{P_{captured}}{S_{incident}} \quad (2.13)$$

$$P_{captured} = \frac{V_{oc}^2}{8R_{rad}}$$

Here  $V_{oc}$  is the open circuit voltage incident on the antenna from the incoming electric field and can be written as  $V_{oc}=E_{inc}l$ . Recalling reciprocity we can also say that captured power depends on  $R_{rad}$  given in eq. 2.6. Therefore,

$$P_{captured} = \frac{(E_{inc}l)^2}{8 \frac{2\pi}{3} Z_o \left(\frac{l}{\lambda}\right)^2} = \frac{3}{8\pi} \left(\frac{E_{inc}^2}{2Z_o}\right) \lambda^2$$

and is independent of length, a strikingly unintuitive result which will be discussed after introducing the Directivity below. The incident flux density is:

$$S_{inc} = \frac{E_{inc}^2}{2Z_o}$$

Therefore the capture cross section is:

$$A_{eff} = \frac{3}{8\pi} \lambda^2 \quad (2.14)$$

We described the voltage seen across the antenna as  $V_{oc}=E_{inc}l$ . This necessarily assumes that the electric field is 1) polarized parallel to the antenna so that the electric field induces movement of charge and 2) the incident radiation is coming from a direction that can be absorbed. For example, as we described earlier a linear upright antenna will not radiate or capture power up or down, parallel with the axis of the antenna. This fact has very real life implications. Car antennas for example receive wavelengths in the FM/AM corresponding to 3-300m and cell phones operate with antennas much shorter than their wavelength of operation which is  $\sim 30$ cm. Despite their size they are able to reliably receive and emit radiation.

For the short dipole, it can only capture power in 2 of the 3 directions. Thus at the direction of maximum radiation it experiences 1.5 times as much power as an ideal equivalent antenna that radiates isotropically. This characteristic is described as directivity and is defined as:

$$D = \frac{S_{max}}{S_{av}}$$

where  $S_{max}$  and  $S_{av}$  are the maximum and average time-average Poynting vector.

$$D = \frac{S_{max}}{\frac{1}{4\pi} \iint_{4\pi} S(R, \theta, \phi) d\Omega}$$

If we factor out  $S_{max}$  we can write this in terms of a normalized radiation intensity  $F_{max}=1$  and  $F(R, \theta, \phi)$ .

$$D = \frac{1}{\frac{1}{4\pi} \iint_{4\pi} F(R, \theta, \phi) d\Omega} = \frac{4\pi}{\Omega_p}$$

where  $\Omega_p$  is the pattern solid angle that the antenna radiates into. For a completely isotropic antenna,  $\Omega_p=4\pi$ . For a short dipole  $D=1.5$ .

In terms of  $D$ , capture cross section for a short dipole results in the following:

$$A_{eff} = \frac{\lambda^2 D}{4\pi} \quad (2.15)$$

This is true in general for any reciprocal antenna, and leads to some surprising results. Namely, the capture cross section of the antenna is roughly independent of antenna size, and as computed before so is the power captured. However, the results from Wheeler tell us to expect higher  $Q_s$  from smaller antennas. The following figure summarizes these results:

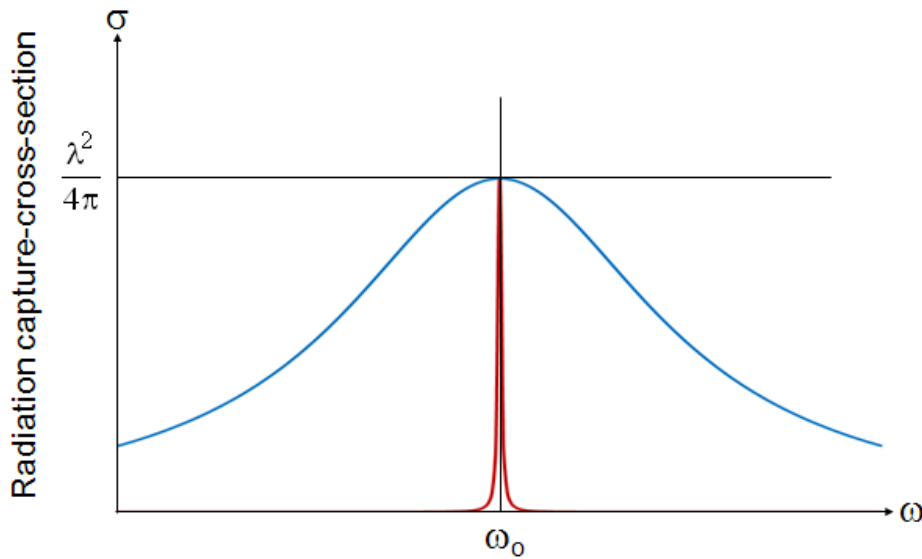


Fig 2.8 The capture cross-section of an electrically short antenna (red) and a long antenna (blue) centered at the same resonance frequency. Note that the peak values are the same, indicating on resonance the captured power by both is equivalent.

We can explain some of this intuitively looking at the circuit model again. At resonance  $\omega = 1/\sqrt{LC}$  and  $j\omega L = 1/j\omega C$ , thus the reactive part is completely canceled out and the voltage is dropped only across the radiation resistance and the load, leading to our conclusion that the power captured is independent of size. However off resonance the voltage is dropped across the reactive part as well. For a high Q structure, a small detuning results in a large decrease in voltage across the load explaining the figure above.

## 2.3 Metal Optics

### 2.3.1 The origin of Kinetic Inductance

At optical frequencies metals behave differently compared to at microwave frequencies. While we can still use the theory presented for optical antennas, these differences cannot be ignored and must be factored into our calculations. At the heart of the issue is kinetic inductance – the inertia of oscillating charges contributing to an additional series inductance in a metal. To see where this comes from consider the relation between conductivity – a traditionally DC and microwave parameter and the permittivity of a material – typically thought of as an optical property.

$$\nabla \times H = J + \frac{dD}{Dt}$$

This can be written completely in terms of a complex permittivity.

$$\nabla \times H = j\omega\epsilon_r(\omega)\epsilon_0 E$$

Equivalently, it can be written in terms of only currents and charges, eliminating the dielectric response:

$$\nabla \times H = \sigma(\omega)E + j\omega\epsilon_0 E$$

Equating the two, gives us the following:

$$\sigma(\omega) = j\omega\epsilon_0(\epsilon_r - 1) \quad (2.16)$$

This complex conductivity is an alternate and completely legitimate form describing currents as well as the dielectric response in any material. The initial separation between the two is arbitrary and mostly due to convention. Usually, the contribution to polarization due to bound charges is lumped into  $\epsilon$  whereas contribution to the current from free charges is described in  $\sigma$ . However, at optical frequencies and especially for metals the distinction between the two is blurred. For the case of a metallic wire the impedance can now be written as:

$$Z = \frac{1}{\sigma(\omega)} \frac{l}{A}$$

As will be described in the next section,  $\sigma(\omega) = nq^2\tau/(m+i\omega m\tau)$ , yielding:

$$Z = \left( \frac{m + j\omega m\tau}{nq^2\tau} \right) \frac{l}{A}$$

$$Z = \left( \frac{m}{nq^2\tau} \right) \frac{l}{A} + j\omega \left( \frac{m}{nq^2} \right) \frac{l}{A}$$

$$Z = R + j\omega L_k \quad (2.17)$$

where  $R$  is the classical DC resistance and  $L_k$  is the inductance due to the inertia of the electron. Due to its  $\omega l/A$  dependence, this inductance becomes important at optical frequencies at the nanometer scale.

### 2.3.2 Drude model

Known as the drude model, the optical properties of metals can be modeled by a free electron gas moving through a lattice of positive ions. The electron cloud oscillates in response to an applied AC electromagnetic field while their motion is damped through collisions with a characteristic rate of  $1/\tau$ . Starting with the equation of motion  $F=ma$ , using  $F=-qE$  and adding in collision we have:

$$-qE(t) = m\ddot{x} + \frac{m}{\tau}\dot{x}$$

where  $x$  is the electrons position. For a field  $E(t)=Ee^{-i\omega t}$ , the solution to  $x$  is:

$$x(t) = \frac{-q}{m\left(\omega^2 + i\frac{\omega}{\tau}\right)}E(t)$$

The oscillating charges create an effective dipole contributing to the macroscopic polarization  $P=-nqx$ , written explicitly as:

$$P = -\frac{nq^2}{m\left(\omega^2 + i\frac{\omega}{\tau}\right)}E$$

The electric flux density  $D=P+\epsilon_0E$  is then yields:

$$D = \epsilon_0 \left( 1 - \frac{nq^2}{m\epsilon_0\left(\omega^2 + i\frac{\omega}{\tau}\right)} \right) E = \epsilon_0 \left( 1 - \frac{\omega_p^2}{\left(\omega^2 + i\frac{\omega}{\tau}\right)} \right) E$$

where  $\omega_p$  is the plasma frequency given by:

$$\omega_p^2 = \frac{nq^2}{\epsilon_0 m} \quad (2.18)$$

Finally we can obtain the frequency dependent complex permittivity of the metal:

$$\epsilon_m(\omega) = 1 - \frac{\omega_p^2}{\left(\omega^2 + i\frac{\omega}{\tau}\right)} \quad (2.19)$$

Splitting this into real and imaginary components  $\epsilon_1$  and  $\epsilon_2$  respectively, we arrive at

$$\begin{aligned} \epsilon_1(\omega) &= 1 - \frac{\omega_p^2}{\omega^2 + \frac{1}{\tau^2}} \\ \epsilon_2(\omega) &= \frac{\omega_p^2 \tau^2}{\omega(1 + \omega^2 \tau^2)} \end{aligned} \quad (2.20)$$

For most metals  $1/\tau \approx 100\text{Thz}$  and at frequencies close to  $\omega_p$ , which is typically in the visible or UV for common metals, the damping is negligible and  $\epsilon_1$  is close to 0. From our everyday experience, we know metals are highly reflective in the visible. This is because the field penetration into the metal is low. At low frequencies  $\epsilon_2$  dominates and the metal is mainly regarded as a good conductor.

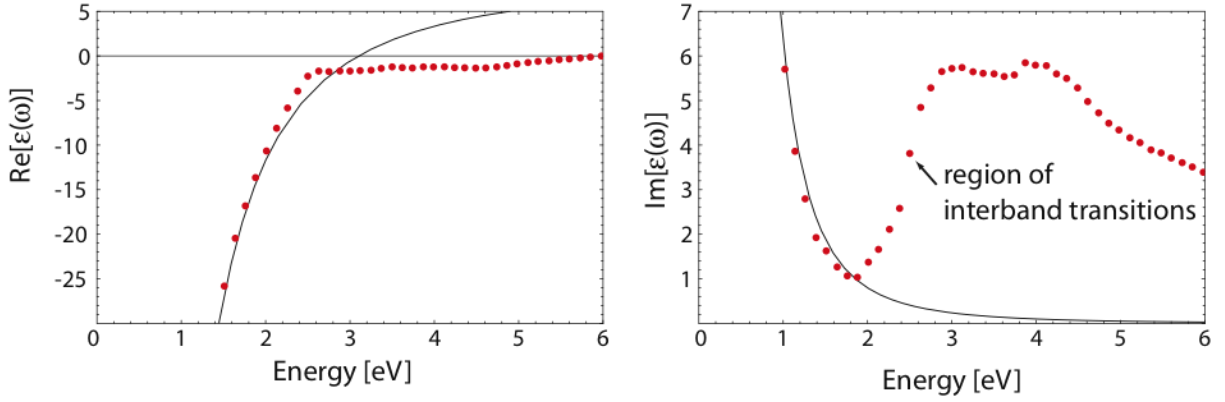


Fig 2.9 The dielectric function of Gold with data from Johnson and Christy. Interband transitions limit the validity of this model at high frequencies [23][24]

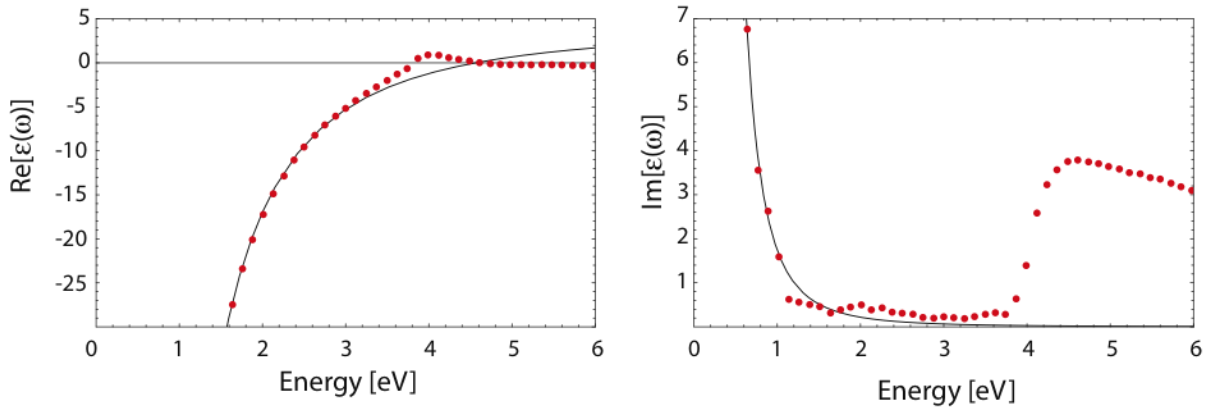


Fig 2.10 The dielectric function of silver with data from Johnson and Christy[23][24].

A consequence of the dielectric function is that in AC, regardless of low or high frequency, there is a skin depth associated with how deep into the metal the electromagnetic field goes. We can derive this quantity recognizing that the refractive index  $n$  is the square root of the permittivity. Doing so yields the following relations:

$$\begin{aligned}\varepsilon_1(\omega) &= n^2 - \kappa^2 \\ \varepsilon_2(\omega) &= 2n\kappa \\ n^2 &= \frac{\varepsilon_1}{2} + \frac{1}{2}\sqrt{\varepsilon_1^2 + \varepsilon_2^2} \\ \kappa &= \frac{\varepsilon_2}{2n}\end{aligned}\tag{2.21}$$

where  $\kappa$  is the extinction coefficient and determines the optical absorption of the electric field through the material. Using the usual harmonic time dependence of electromagnetic waves, this is linked to the absorption coefficient of intensity (i.e.  $I(x)=I_0e^{-\alpha x}$ ) by:

$$\alpha(\omega) = \frac{2\kappa(\omega)\omega}{c} \quad (2.22)$$

This relation can also be used to define a skin depth over which the field decays into the metal to 1/e its initial value (i.e.  $E(z)=E_0e^{-z/\delta}$ )

$$\delta(\omega) = \frac{2}{\alpha(\omega)} \quad (2.23)$$

This model is valid as long as the mean free path of the electron is less than the skin depth. For gold at optical frequencies this skin depth tends to be ~25nm or so and the mean free path of the electron is ~10nm. This mean free path is heavily dependent on grain boundaries as well as corners. For the case that this isn't satisfied (potentially optical antennas), the anomalous skin effect must be taken into account which can increase the losses in an antenna [25].

## 2.4 Spontaneous emission rate Enhancement

### 2.4.1 Quantum Mechanical Description of Spontaneous emission

One very interesting characteristic of spontaneous emission, unlike stimulated emission, is that its rate is dependent on the electromagnetic environment. We can see this arising from Fermi's golden rule for a 2 level system between electronic states m and n:

$$\frac{1}{\tau_{sp}} = \frac{2\pi}{\hbar} |\langle m | q\mathbf{x} \cdot \mathbf{E} | n \rangle|^2 \frac{dN}{dE} \quad (2.24)$$

Where  $dN/dE$  is the photonic density of states i.e the number available photon states per energy level. For free space, we can assume a large 3D box with sides of length L in which the photon must reside as a standing wave. Since, the solution to this requires  $\sin(kL)=0$ , the electromagnetic wave=vector k must be an integer multiple of  $\pi/L$ . Now we can approximate the number of modes in k-space as sphere in k space divided by the spacing between each mode. We restrict ourselves to only positive values of k and multiply by 2 to account for both polarizations:

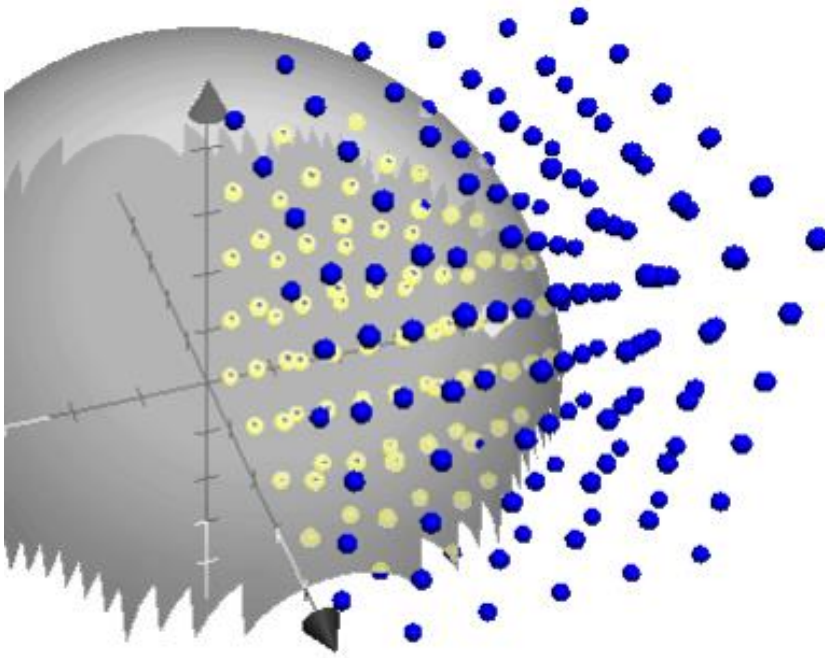


Fig 2.11 Blue points represent states in k-space while the points inside the sphere represent the total number of states for a given energy.

$$N(k) = \frac{\frac{4}{3}\pi k^3 * 2 * \frac{1}{8}}{\left(\frac{\pi}{L}\right)^3}$$

We also know that  $E = \hbar\omega$  and  $\omega = ckn$ , and so  $k = nE/\hbar\omega$ . Rewriting as a function of E:

$$N(E) = \frac{1}{3} \frac{n^3 E^3 V}{\pi^2 \hbar^3 c^3}$$

where V is the volume of the box. Now we take the derivative with respect to E to get the photon density of states and rewrite it in terms of  $\omega$ .

$$\frac{dN}{dE} = \frac{n^3 \omega^2 V}{\hbar c^3 \pi^2} \quad (2.25)$$

Calculating the matrix element in this system requires 2<sup>nd</sup> quantization, which involves quantizing the electromagnetic field subject to normalization. Doing so gives us the electric field:

$$\mathbf{E} = i \sqrt{\frac{\hbar\omega}{2\varepsilon V}} (\mathbf{a}^\dagger e^{-i\mathbf{k}\cdot\mathbf{r}-i\omega t} + \mathbf{a} e^{i\mathbf{k}\cdot\mathbf{r}-i\omega t}) \hat{\mathbf{e}}$$

where  $\mathbf{a}^\dagger$  and  $\mathbf{a}$  are the raising and lowering operators for photon states respectively and  $V$  is the volume. The polarization is represented by  $\hat{\mathbf{e}}$ . Evaluating the matrix element using the raising and lowering operators gives us:

$$|\langle \mathbf{x} \cdot \mathbf{E} \rangle|^2 = |\langle \mathbf{a}^\dagger + \mathbf{a} \rangle|^2 \hbar\omega / 2n^2\varepsilon_0 V$$

The dot product between the vectors yields a cosine and when averaged over solid angle gives 1/3. This is also equivalent to averaging over polarizations. If we consider the case that state  $m$  has 1 photon and state  $n$  has none, the spontaneous emission rate from Fermi's golden rule is then

$$\frac{1}{\tau_{sp}} = \frac{2\pi}{3\hbar} |\langle 1, m | q\mathbf{x}(\mathbf{a}^\dagger + \mathbf{a}) | 0, n \rangle|^2 \frac{\hbar\omega}{2n^2\varepsilon V} \frac{n^3\omega^2 V}{\hbar c^3 \pi^2}$$

Remembering that the raising and lowering operators act only on photon states,  $\langle 1, m | (\mathbf{a}^\dagger + \mathbf{a}) | 0, n \rangle = 1$  and rearranging terms we arrive at:

$$\frac{1}{\tau_{sp}} = \frac{n\omega^3}{3\pi c^3 \varepsilon_0 \hbar} \cdot |q\mathbf{x}|^2 \quad (2.26)$$

This spontaneous emission rate is correct for a 2-level system such as that in an atom or molecule in the weak coupling regime in an infinite homogenous medium. For semiconductor with a continuum of bands, we must take into account the electronic density of states, which will be detailed in the next section. Comparing this to the result we got classically for a short radiating dipole in eq. 2.5 we see that it only produces half of the rate computed by the quantum mechanical treatment because in eq 2.26 the position is spatially averaged. The other half is due to vacuum fluctuations or radiation reaction, essentially the field emitted by the dipole exerted on itself. [26]The details on this are available in appendix 2.

## 2.4.2 The Purcell Effect

Now imagine that rather than emitting into free space, the spontaneous emission is radiating into a cavity with only 1 mode. Purcell first calculated this in 1946 and his result is derived below[27]. Again we start with Fermi's golden rule, but consider the case where there is only 1 available photon mode into a finite energy interval  $\hbar\Delta\omega$ . First we must correctly normalize this new density of states i.e. integrating over energy must yield 1 photon mode.

$$\int_0^\infty \frac{dN}{dE} dE = 1$$

Assuming a Lorentzian lineshape the normalization condition is satisfied when,

$$\frac{dN}{dE} = \frac{2}{\pi\hbar\Delta\omega} \frac{\hbar\Delta\omega^2}{4\hbar(\omega - \omega_c)^2 + \hbar\Delta\omega^2} \quad (2.27)$$

where  $\omega_c$  is the resonance frequency of the cavity. If  $\omega = \omega_c$  we arrive at:

$$\frac{dN}{dE} = \frac{2}{\pi\hbar\Delta\omega} \quad (2.28)$$

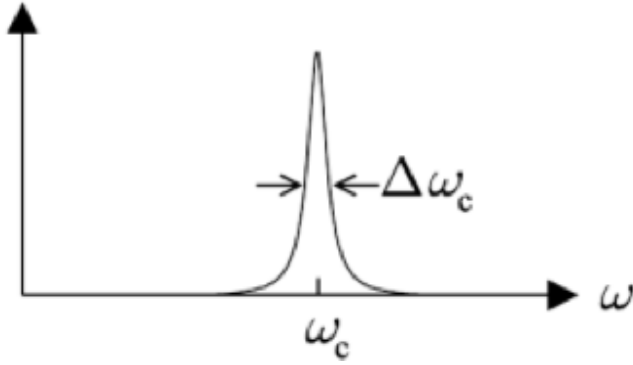


Fig 2.12 The density of states function  $dN/dE$  for the cavity. The frequency of the mode is  $\omega_c$  and the FWHM is  $\Delta\omega$

Plugging this into fermi's golden rule we have

$$\frac{1}{\tau_{sp}} = \frac{2\pi}{\hbar} |\langle m | q\mathbf{x} \cdot \mathbf{E}_{max} | n \rangle|^2 \frac{2}{\pi\hbar\Delta\omega}$$

where  $E_{max}$  is the maximum electric field in the cavity exciting the transition. The zero-point field is the driving force behind the emission so necessarily the energy in the cavity must be equivalent to  $\hbar\omega/2$ .

$$\int \epsilon E^2 dV = \frac{\hbar\omega}{2}$$

Then we can normalize the effective volume in the following way:

$$V_{eff} = \frac{\int \epsilon E^2 dV}{\epsilon E_{max}^2} \quad (2.29)$$

Doing so allows us to write  $E_{max}$  as a function of  $V_{eff}$ , very similar to the result that would have been obtained in 2<sup>nd</sup> quantization of a free electric field.

$$E_{max}^2 = \frac{\hbar\omega}{2\epsilon V_{eff}}$$

The spontaneous emission rate in a cavity is now given and recognizing that the cavity Q is simply  $\omega/\Delta\omega$  we have:

$$\frac{1}{\tau_{sp}} = \frac{2\pi}{\hbar} |qx|^2 \frac{\hbar\omega}{2\varepsilon V_{eff}} \frac{2}{\pi\hbar\Delta\omega}$$

$$\frac{1}{\tau_{sp}} = \frac{2}{\hbar\varepsilon} |qx|^2 \frac{Q}{V_{eff}} \quad (2.30)$$

Dividing by the rate of spontaneous emission in free space, we arrive at the Purcell factor or the rate enhancement of spontaneous emission due to a cavity:

$$F = \frac{1}{\tau_{sp,c}} / \frac{1}{\tau_{sp,free\ space}}$$

$$F = \frac{3}{4\pi^2} \frac{Q(\lambda/n)^3}{V_{eff}} \quad (2.31)$$

Clearly the rate enhancement of spontaneous emission is dependent on  $Q/V_{eff}$ , however we must be careful since a high quality factor will also trap photons inside the cavity. If the goal is to increase the total rate of emission from the cavity, the Q cannot be so high that the photons are not released. Therefore, recognizing that the cavity bandwidth is equivalent to 1 over the decay time,  $1/\tau_{sp} = 1/\tau_{cav} = \Delta\omega_{cav}$  for the fastest rate of emission. A faster rate of spontaneous emission rate will put us in the strong coupling regime where fermi's golden rule no longer applies. Applying this to eq (2.30):

$$\frac{1}{\tau_{sp,opt}^2} = \frac{2}{\hbar\varepsilon} |qx|^2 \frac{\omega}{V_{eff}}$$

We can subdivide this into parts as follows:

$$\frac{1}{\tau_{sp,opt}^2} = \frac{q^2}{4\pi\varepsilon_0\hbar c} \frac{2 * 4\pi c\omega|x|^2}{\varepsilon_r V_{eff}}$$

The term in front is the fine structure constant  $\alpha \approx 1/137$

$$\frac{1}{\tau_{sp,opt}} = \sqrt{\alpha} \sqrt{\frac{4\omega^2|x|^2\lambda n}{\varepsilon_r V_{eff}}}$$

$$\frac{1}{\tau_{sp,opt}} = 2\omega\sqrt{\alpha} \sqrt{\frac{|x|^2\lambda}{nV_{eff}}}$$

which gives us the optimal Q for a given cavity size:

$$Q_{opt} = \frac{\omega}{\frac{1}{\tau_{sp,opt}}} = \frac{1}{2\sqrt{\alpha}} \sqrt{\frac{nV_{eff}}{|x|^2\lambda}} \quad (2.32)$$

Thus the maximum spontaneous emission rate from a cavity is dependent on  $\omega$  as well as a volume factor. The optimal  $Q$  gives us a clue as to the type of structure that is needed for this rate. For example, for high  $Q$  cavities such as photonic crystals, the effective volume is quite large  $\sim(\lambda/2n)^3$ , but the  $Q$  can be extremely high  $\sim 10^6$ . Merely looking at the equation given by the Purcell effect would lead you to conclude that it could enhance the rate by 5 or 6 orders of magnitude. However, using  $Q_{opt}$  we see that without going into strong coupling, we get a net enhancement of only 2 to 3 orders of magnitude. On the other hand optical antennas can have moderate  $Q$ s and very low effective volumes, reaching 6 or even 7 orders of magnitude in rate enhancement. The analysis of this will be given in the next section.

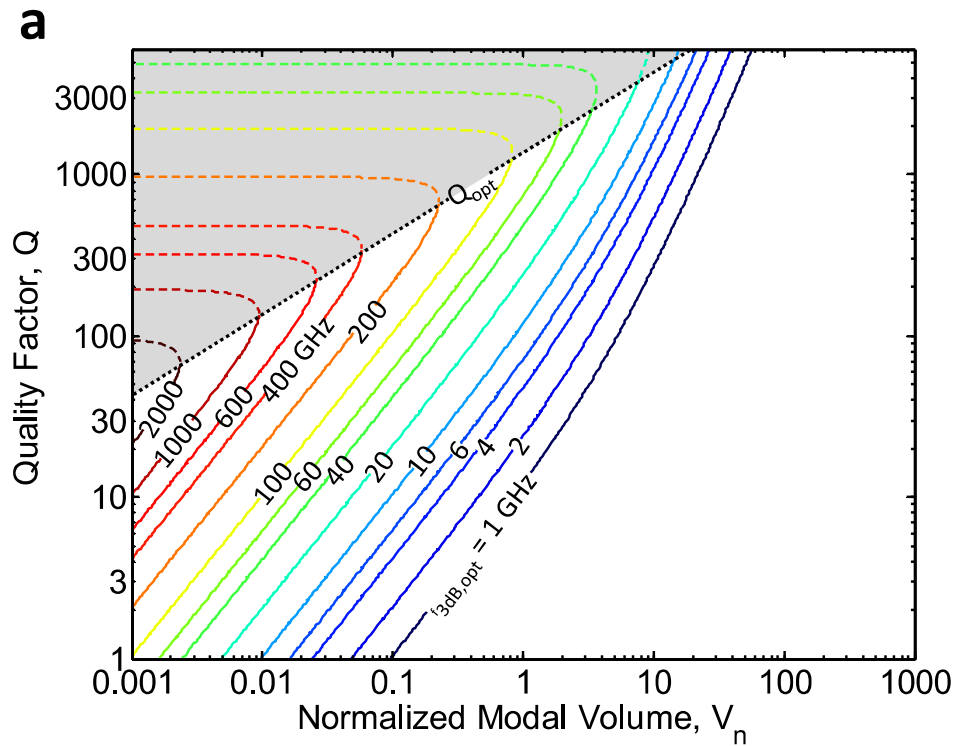


Fig 2.13 Contour plots of modulation speed as a function of  $V_n = V_{eff}/(\lambda/2n)^3$  and  $Q$ . The optimal  $Q$  is on the border of the shaded region and white region which represents the transition to strong coupling [28].

### 2.4.3 Optical Antenna assisted spontaneous hyper emission

To see how an optical antenna enhances the spontaneous emission rate consider a dipole oscillating in the gap of an antenna.

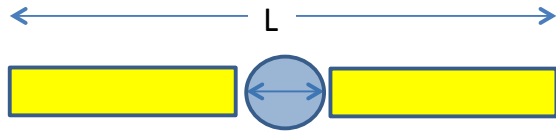


Fig 2. Dipole at the feedgap of an antenna with currents oscillating parallel to the long axis of the antenna

In the simplest model, the dipole acts as a current source with  $I=q\omega x_o/d$  as given by the Shockley-Ramo theorem[29][30] upon the leads of the antenna, where  $x_o$  is the dipole length and  $d$  is the gap distance. The power output is still  $I^2 R_{rad}/2$  and dividing by the energy of a photon,  $\hbar\omega$  we arrive at the rate of emission due to the dipole coupled antenna:

$$\frac{P}{\hbar\omega} = \frac{1}{\tau_{ant}} = \frac{1}{2\hbar\omega} \left(\frac{q\omega x_o}{d}\right)^2 R_{rad}$$

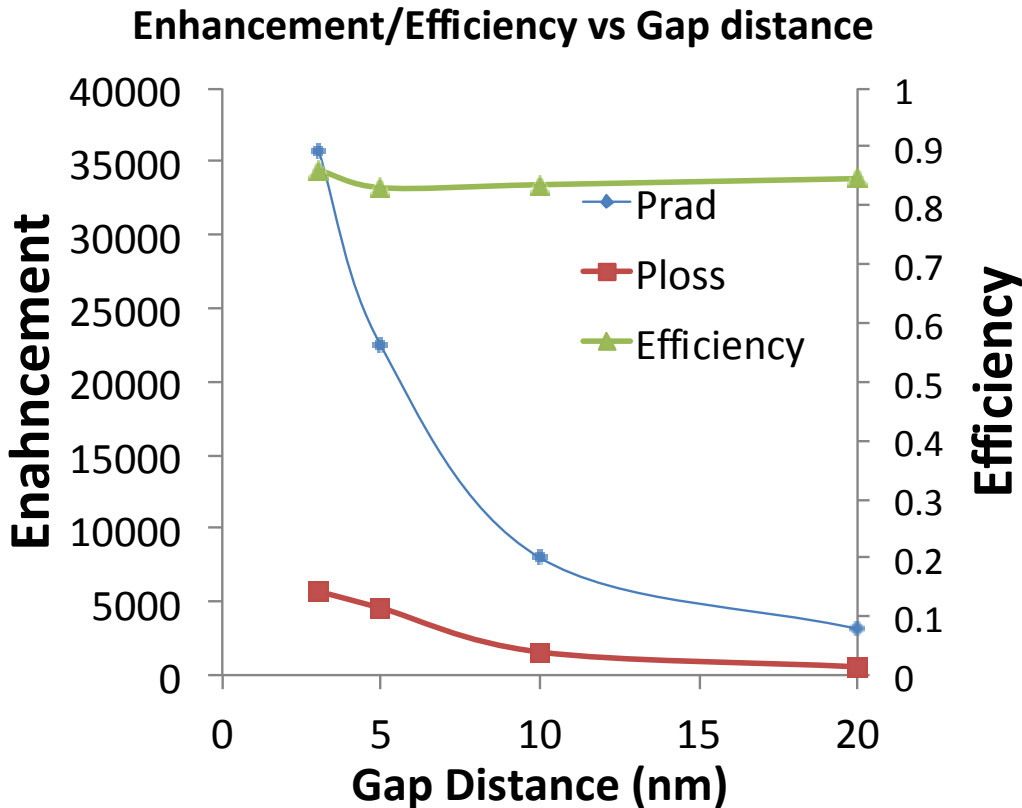


Fig 2.14 Simulations using CST Microwave studio of Enhancement vs gap distance. The emission wavelength was kept fixed at 1300nm and  $Q \sim 8$ . The efficiency is roughly constant when using a gold data from Johnson and Cristy.

The ratio of  $1/\tau_{ant}$  to  $1/\tau_{dipole}$  is the rate enhancement factor.

$$\frac{1/\tau_{ant}}{1/\tau_{dipole}} = \frac{\frac{1}{2} \left( \frac{q\omega x_o}{d} \right)^2 R_{rad}}{\frac{\pi}{3\hbar\omega} Z_o \left( \frac{x_o}{\lambda} \right)^2 (q\omega/2)^2}$$

$$\frac{1/\tau_{ant}}{1/\tau_{dipole}} = \frac{3}{2\pi} \frac{R_{rad}}{Z_o} \left( \frac{\lambda}{d} \right)^2$$

Depending on the specifics of the wavelength chosen, the gap spacing and the antenna design, this enhancement can be in the 100s and even 1000s potentially reaching Thz regime modulation. For some specific numbers we can plug in the radiation resistance due to a short antenna of length  $l$ , given below

$$R_{rad} = \frac{\pi}{6} Z_o \left( \frac{l}{\lambda} \right)^2$$

Comparing the equation above to the radiation resistance of a hertzian dipole (eq2.6), we notice that it is exactly 4 times less. This is due to the non-uniform current distribution along the leads. The total rate is now:

$$\frac{P}{\hbar\omega} = \frac{1}{\tau_{ant}} = \frac{1}{2} \left( \frac{q\omega x_o}{d} \right)^2 \frac{\pi}{6\hbar\omega} Z_o \left( \frac{l}{\lambda} \right)^2$$

And the enhancement after much cancellation is:

$$\frac{1/\tau_{ant}}{1/\tau_{dipole}} = \frac{1}{4} \left( \frac{l}{d} \right)^2$$

Note for all these cases, the enhancement and rate are due to a correctly oriented dipole. If the dipoles are randomly oriented, then the enhancement must be divided by a factor of 3.

#### 2.4.4 Relating Purcell Enhancement to Antenna Enhancement

We have seen two different ways by which the spontaneous emission rate can be enhanced. The two can be related by finding an effective volume of the antenna. From before the definition of effective volume is:

$$\epsilon E_{max}^2 V_{eff} = \int \epsilon E^2 dV$$

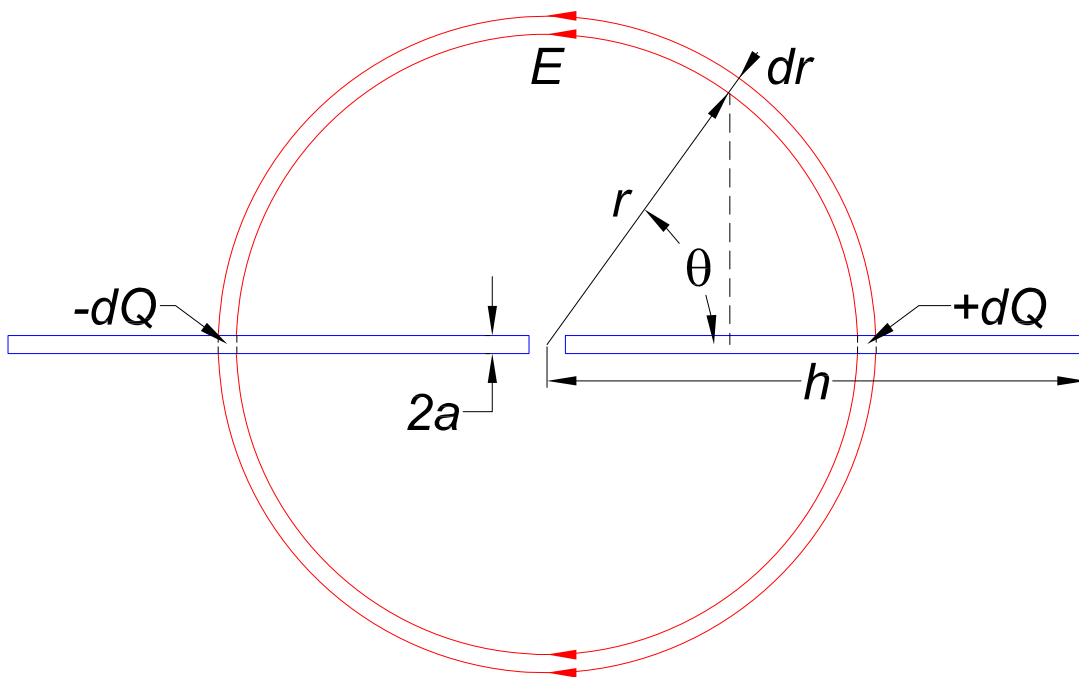
For a short antenna this energy is stored in the capacitance. The feed gap provides a capacitance of  $C_{gap} = \epsilon A/d$ , where  $A$  is the cross sectional area of the antenna and  $d$  is the gap spacing. Since the antenna arms are good conductors we can assume that most of voltage falls directly across the gap and therefore  $E_{max}$  is the electric field in the gap. Rewriting this in terms of capacitance then gives us:

$$\frac{1}{2} \frac{C_{gap} V^2}{Ad} V_{eff} = \frac{1}{2} C_{total} V^2$$

On the right we have divided the total energy stored in the gap capacitance by the volume of gap to find the energy density. Solving for  $V_{eff}$  yields,

$$V_{eff} = \frac{C_{total}}{C_{gap}} Ad$$

The total capacitance of any linear conductor will typically be proportional to  $\epsilon \times$  length with some factor on bottom dependent on only a natural log of the dimensions. For a more detailed model that yield very similar results, we can assume that the field lines from a charge  $dQ$  (in interval  $dr$ ) on one arm follow a semicircular path to the opposite charge on the other arm.



If so, all the field lines emanating from charge  $dQ$  in interval  $dr$  at distance  $r$  from the charge are enclosed in the Gaussian surface. Fig 2.15 An approximation to electric field lines emanating from a short dipole antenna.

Drawing a Gaussian surface over only the field lines enclosed in a solid half-angle  $\theta$ , encloses only the charge  $dQ$ . The electric field is then

$$E = \frac{dQ}{2\pi\epsilon_0 r \sin\theta dr}$$

Now integrating over one semicircular path gives us the voltage:

$$V = 2 \int_{\theta_{min}}^{\pi/2} E r d\theta = \frac{dQ}{dr\pi\epsilon_o} \int_{a/r}^{\pi/2} \frac{d\theta}{\sin\theta} = \frac{dQ}{dr\pi\epsilon_o} \ln\left[\tan\left(\frac{\theta}{2}\right)\right]_{a/r}^{\pi/2}$$

$$V = \frac{dQ}{dr\pi\epsilon_o} \ln\left[\frac{2r}{a}\right]$$

Above we have taken the charge density as roughly constant along the length, which is a reasonable approximation for short antennas. However, the voltage difference between the two arms should not be dependent on the path taken, which is an artifact from the model. Since the voltage is only dependent on the natural log though, we can take average value and set  $r=l/4$ . Doing so and dividing by  $dQ$  gives us the capacitance per unit length:

$$dC = \frac{\pi\epsilon_o dr}{\ln\left(\frac{l}{2a}\right)}$$

Finally,

$$C_{ant} = \frac{\pi\epsilon_o l}{2\ln\left(\frac{l}{2a}\right)} = \epsilon_o l_c$$

where  $l_c$  is an effective capacitive length which as mentioned earlier is roughly  $\epsilon_o l$ . If we go back and compute  $V_{eff}$  now with  $a=d$  and  $l_c \gg a$ ,  $C_{ant}=C_{total}$ ,

$$V_{eff} = \frac{\epsilon_o l_c}{\epsilon_o a^2/d} a^2 d = l_c d^2$$

which is approximately the physical volume of the entire antenna. We can relate this to the Purcell effect, by noting that  $Q=\omega R_{total} C_{total}$  in an parallel RLC circuit. In the absence of losses,  $R_{total} = R_{rad}$  and  $1/\tau = 1/\tau_{ant}$

$$\frac{1}{\tau} = \frac{1}{2\hbar\omega} \left(\frac{q\omega x_o}{d}\right)^2 R_{total}$$

$$\frac{1}{\tau} = \frac{1}{2\hbar\omega} \left(\frac{q\omega x_o}{d}\right)^2 \frac{Q}{\omega C_{total}}$$

Now using  $C_{total} = V_{eff} C_{gap}/Ad$  and rearranging terms we arrive at:

$$\frac{1}{\tau} = \frac{(qx_o)^2}{2\hbar\epsilon_o} \frac{Q}{V_{eff}}$$

which is off by a factor of 4 from the Purcell effect probably due to time/spatial averaging and the aforementioned vacuum fluctuations/radiation reaction.

## 2.4.5 Enhanced Modulation Speed

As alluded to in chapter 1, the photon decay rate is responsible for the maximum speed of modulation in a device. To understand the carrier dynamics behind this we provide the rate equation for an LED, with carrier density  $N$ .

$$\frac{dN}{dt} = G_{gen} - (R_{sp} + R_{nr} + R_{leakage} + R_{st})$$

where  $G_{gen}$  is the generation rate of carriers from electrical or optical pumping, while  $R_{sp}$  is the spontaneous emission rate,  $R_{nr}$  is the non-radiative recombination rate,  $R_{leakage}$  is the leakage due to diffusion and  $R_{st}$  is the stimulated emission rate. In the absence of a large photon density as will be the case for an optical antenna  $R_{st}$  is small and can be neglected. We can now rewrite this equation with its dependence on  $N$  that these rates have.

$$\frac{dN}{dt} = G_{gen} - (BN^2 + AN + CN^3) - R_{st}$$

Though these rates will have a non-exponential decay it is convenient to lump these parameters into a radiative efficiency  $\eta_r(N)$  and a characteristic carrier lifetime  $\tau(N)$  so that we can obtain a simpler picture of the carrier dynamics.

$$\eta_r(N) = \frac{R_{sp}}{R_{sp} + R_{nr} + R_{leakage}}$$

$$\frac{dN}{dt} = -\frac{N}{\tau(N)} = -(BN^2 + AN + CN^3)$$

where we have neglected the steady state  $G_{gen}$  to find a decay rate with initial population  $N_i$ . The cubic term represents Auger recombination, which may be negligible under lower levels of injection. If the term  $AN$  is dominant then the solution to this is:

$$N(t) = N_i e^{-t/\tau}$$

for which the frequency response is:

$$N(\omega) = \frac{N(0)}{1 + j\omega\tau}$$

As above and in general, decreasing the carrier lifetime, increases the modulation bandwidth. This can be achieved simply by increasing the non-radiative rate, effectively lowering the efficiency – a suboptimal solution with the obvious tradeoff. Enhancing spontaneous emission with an optical antenna; in contrast, simultaneously decreases the carrier lifetime and increases the efficiency.

## 2.4.6 Spontaneous emission rate enhancement from a semiconductor

Relating this to a semiconductor, we note that in addition to an optical density of states there is an electronic density of states. We first start with the equation for the rate of absorption per volume given by fermi's golden rule in a 2-level system.

$$R_{abs} = \frac{2\pi}{\hbar} |qx_o E|^2 \delta(E_2 - E_1 - \hbar\omega)$$

where the delta function is to satisfy energy conservation. Due to the fact there are a continuum of states in both the conduction and the valence band in a semiconductor the delta function becomes:

$$r_{abs}(\hbar\omega) = \frac{2\pi}{\hbar} |qx_o E|^2 \rho_r(\hbar\omega) (f_c - f_v)$$

Here I've used the lower case r to describe the absorption rate per unit energy. The reduced 3D density of electronic states is  $\rho_r$  and incorporates the states due to both bands given below:

$$\rho_r(\hbar\omega) = \frac{1}{2\pi^2} \left( \frac{2m_r^*}{\hbar^2} \right)^{3/2} \sqrt{\hbar\omega - Eg}$$

The  $f_c$  and  $f_v$  are the distributions of electrons and holes respectively due to the quasi-Fermi levels, given below:

$$f_c = \frac{1}{1 + e^{(E_c - F_c)/kT}} \quad f_v = \frac{1}{1 + e^{(E_v - F_v)/kT}}$$

We can express this in terms the absorption coefficient which has units of  $\text{cm}^{-1}$ , by dividing by the incoming photon flux  $S = \epsilon c |E|^2 / 2n\hbar\omega$ .

$$\alpha(\hbar\omega) = \frac{\pi\omega}{n\epsilon_o c} |qx_o|^2 \rho_r(\hbar\omega) (f_c - f_v)$$

Similarly,

$$r_{spont}(\hbar\omega) = \frac{2\pi}{\hbar} |qx_o E|^2 \rho_r(\hbar\omega) \rho_{photon}(\hbar\omega) f_c (1 - f_v)$$

Again the spontaneous emission rate is dependent on the photon density of states and integrating over energy gives us the total rate. By matching the emission frequency with the cavity frequency it is apparent that the peak rate is enhanced by the Purcell factor.

## Chapter 3: Design and Fabrication

To test the theory outlined in the previous 2 chapters, optical antennas were fabricated on the quaternary semiconductor InGaAsP. InGaAsP is typically used as a laser gain material for communications applications in the infrared and its emission wavelength can be tuned in the range of 1000nm to 1680nm based upon the alloy concentration. Phosphide based materials are attractive for use in nano-scale devices where the surface to volume ratio is large, as their surface recombination tends to be lower. For example InP bulk has a surface recombination velocity of  $<10^4$  cm/s while GaAs is more than an order of magnitude higher at  $\sim 5 \times 10^5$  cm/s. This wavelength also allows for reasonable fabrication as length scales are in the  $\sim 100$ s of nm which can be achieved with photolithography.

We know that increasing the density of states increases the spontaneous emission and so that as a proof of concept a simple cavity or antenna will work. The simplest antenna structure is just a metal bar which has a resonance frequency dependent upon its dimension. Placing this in the on the semiconductor material allows the dipoles to couple to the ends and thus radiate. Gold is a commonly used material in this wavelength regime known for its low loss and while silver is less lossy, it is easily oxidized and so was not considered for ease of fabrication. However, future structures may want to incorporate silver with a capping layer of gold to increase efficiency.

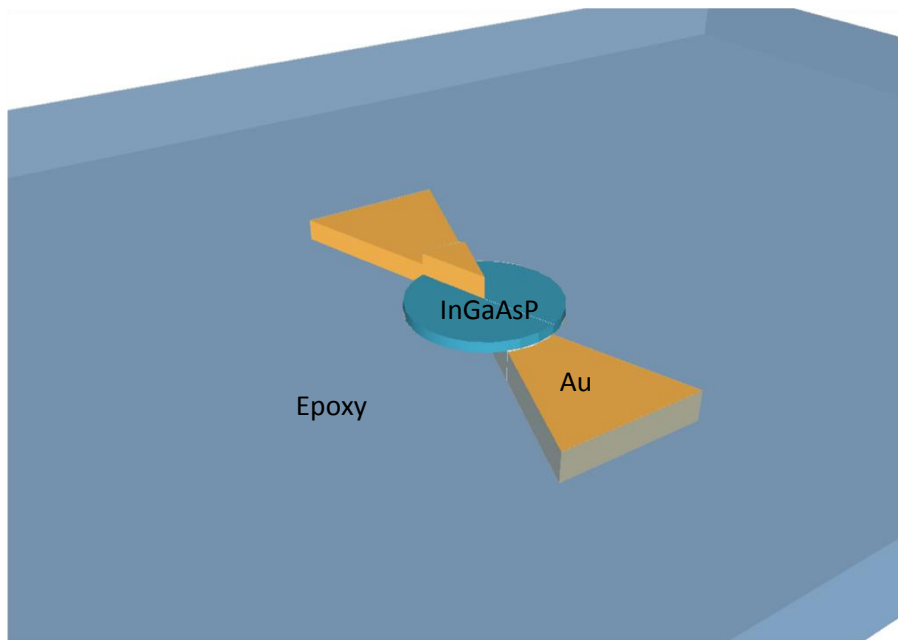


Fig 3.1 Bowtie antenna coupled to a patch of InGaAsP

From our analysis in chapter 2, the most effective antenna is one with a small feedgap, but also small cross sectional area to reduce the capacitance of the gap in the circuit model and reduce the

overall effective volume from the viewpoint of the Purcell effect. To this end we chose a bowtie antenna with the InGaAsP sandwiched between them shown in figure 3.1. Additional rectangular wide antennas (fat dipoles) were fabricated to aid in alignment. The thickness of the InGaAsP layer is very well defined by epitaxial growth and not lithography so very small feedgaps can be made.

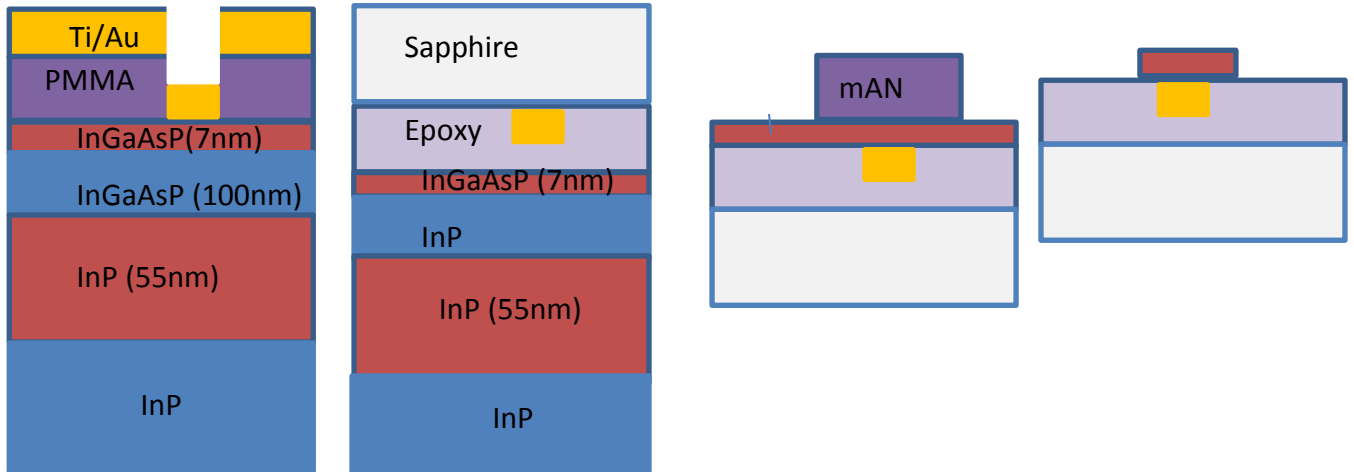


Fig 3.2. Fabrication procedure: 1. Spin on PMMA, Electron Beam Lithography, metal deposition 2. Liftoff, Flip Chip to Sapphire handle with epoxy, substrate removal 3. Spin mAN, etch and resist removal.

### 3.1 Bar Antenna Fabrication

The fabrication for the single-sided antenna structure starts with an epitaxially grown layer of 25nm InP/7-20nm InGaAsP/55nm InP/100nm on an InP substrate. The InP epitaxial layer on top is to prevent oxidation of the InGaAsP and on the back is to prevent over-etching when removing the substrate. The First the InP buffer on top is etched using a HCl:H<sub>3</sub>PO<sub>4</sub> (1:1) etch for 10s rinsed in DI water and baked at 150C at 1min to remove any residual water. A negative e-beam resist, PMMA A-2, is then spun at 2000RPMs for 45s and baked at 185degrees for 90s to evaporate the solvents. Electron beam lithography defines arrays of rectangles with different lengths, which is then developed in MIBK:IPA(1:3) for 60s. Titanium (3nm) and gold (25nm) are deposited by e-beam evaporation and lift-off is done with acetone for a few minutes. The Ti is used as an adhesive layer as well as a barrier to prevent Au diffusion into the InGaAsP layer. The sample is then epoxied face down onto a sapphire carrier with Norlands optical adhesive NOA-81(refractive index=1.5) , baked in a UV oven for 10 mins and then on a hotplate for 12 hours at 150C for a full cure. The InP substrate is then grinded down ~100um using a lapping tool and sandpaper. The residual InP is etched in HCl:H<sub>3</sub>PO<sub>4</sub> (1:1) at 70C for ~ 30mins which is highly selective and stops at the InGaAsP etch stop. The InGaAsP is then etched with

$\text{H}_2\text{O}:\text{H}_2\text{O}_2:\text{H}_2\text{SO}_4$  (1:1:10) which is highly selective against InP. Finally the InP buffer layer is etched in  $\text{HCl}:\text{H}_3\text{PO}_4$  (1:1) to reveal the InGaAP quantum well.

InGaAsP further from the metal nanorods will not couple to the antenna and thus when testing the device this excess material will show up as background signal and drown out signal from the antenna. Therefore, it must be etched away to provide signal only from the antenna. First a monolayer of HMDS is deposited for adhesion in an HMDS oven. A positive e-beam resist, maN-2403, is spun on at 3000 RPMs for 30s and baked at 90C for 60s yielding a resist thickness of ~300nm. To prevent charging during the subsequent e-beam exposure a conductive polymer, Aquasave, is spun on at 3500 RPMs for 30s and baked at 110C for 30s. Using registration marks defined on the first metal deposition, circular patches are exposed directly on top of the InGaAsP for use as a hardmask. The maN-2403 is then developed in 10% TMAH in water for 60s and the InGaAsP layer is etched in  $\text{H}_2\text{O}:\text{H}_2\text{O}_2:\text{H}_2\text{SO}_4$  (1:8:500) for 10s as this solution etches at ~1nm/s.

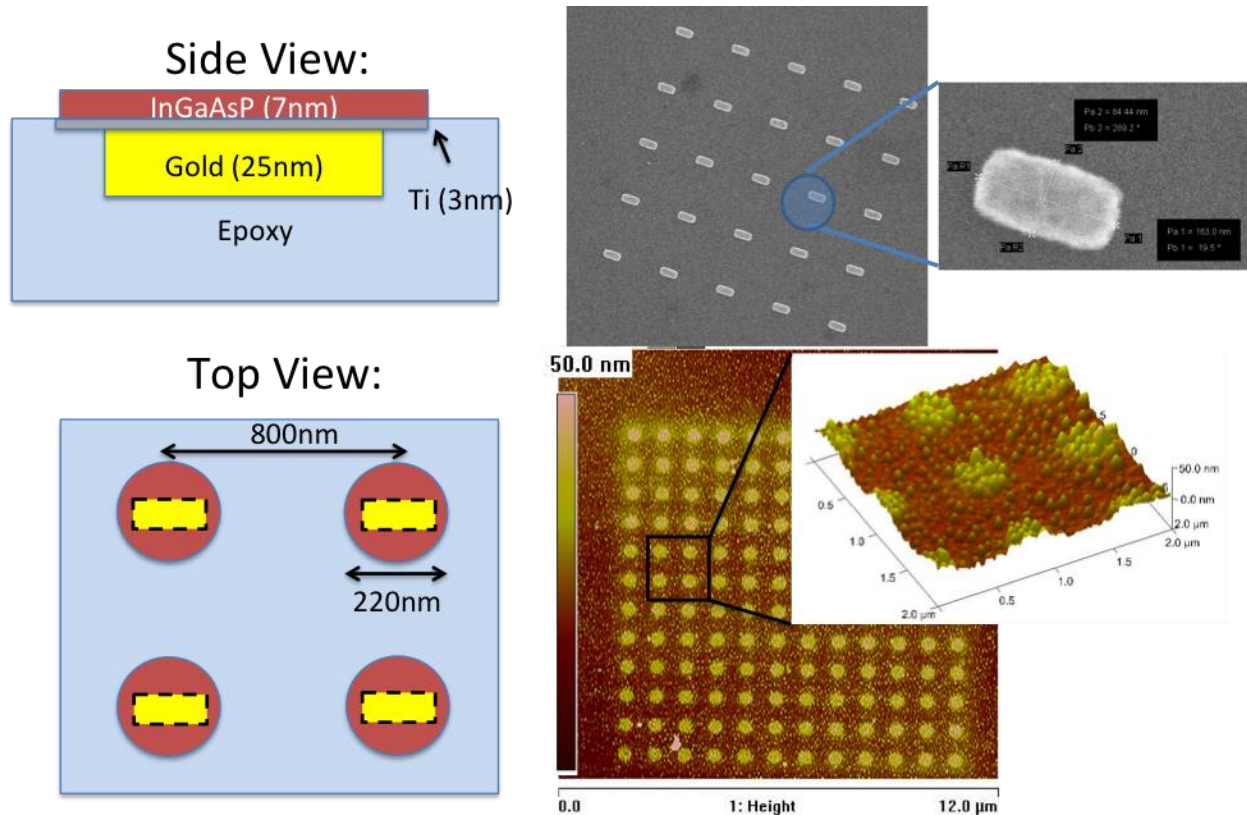


Fig3.3. The schematics show the fabricated device. SEM images were taken before InGaAsP patch definition to prevent charging. AFM images are taken after the etch.

Arrays of devices were fabricated with 220nm and 350nm patches and different antenna lengths. As a control patches with no antennas and patches with misaligned antennas were made adjacent to test arrays. Within the array, devices are spaced greater than half a wavelength apart (800nm)

to prevent coupling of the antennas. The testing methods and experimental observations and discussion will be discussed in the next chapter.

### 3.2 Bowtie Antennas and Fat dipole Fabrication

The same basic concept was applied to bowtie antennas and wide antennas. An extra e-beam alignment and mask was designed to overlay on the existing half-antenna and patches creating. Following the same procedure as before for e-beam lithography using PMMA A-2, exposure and metal deposition, the full structure was fabricated seen in Fig3.4.

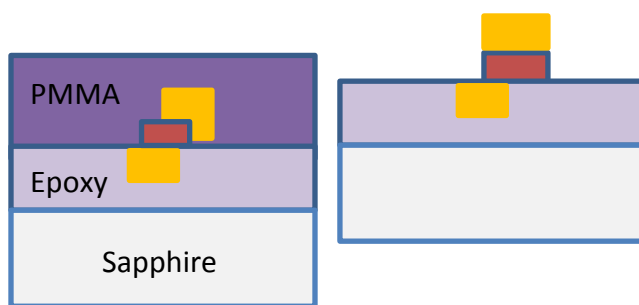
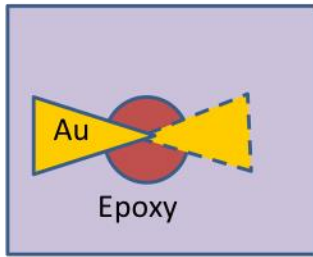


Fig 3.4 Continuing from fig 3.3, 4. Spin PMMA, EBL 5. Metal deposition

The alignment accuracy for fabricated structures is nominally 10nm on the e-beam lithography tool, however combining charging effects from the underlying oxide as well as thickness variations from the epoxy this can span up to 50nm. For this reason, arrays are intentionally misaligned in 25nm increments both laterally and vertically to achieve reasonable alignments on at least some of the arrays. Ideally the InGaAsP etch mask would not require alignment(as done so with the circular patch) as it can be masked by the antenna arms; however doing so creates difficulty in testing as the pumping and emission of the etched area is greatly weakened. Note that on the top down SEMs one of the antenna arms is actually beneath the patch of InGaAsP and imbedded in epoxy.

Top View



Side View

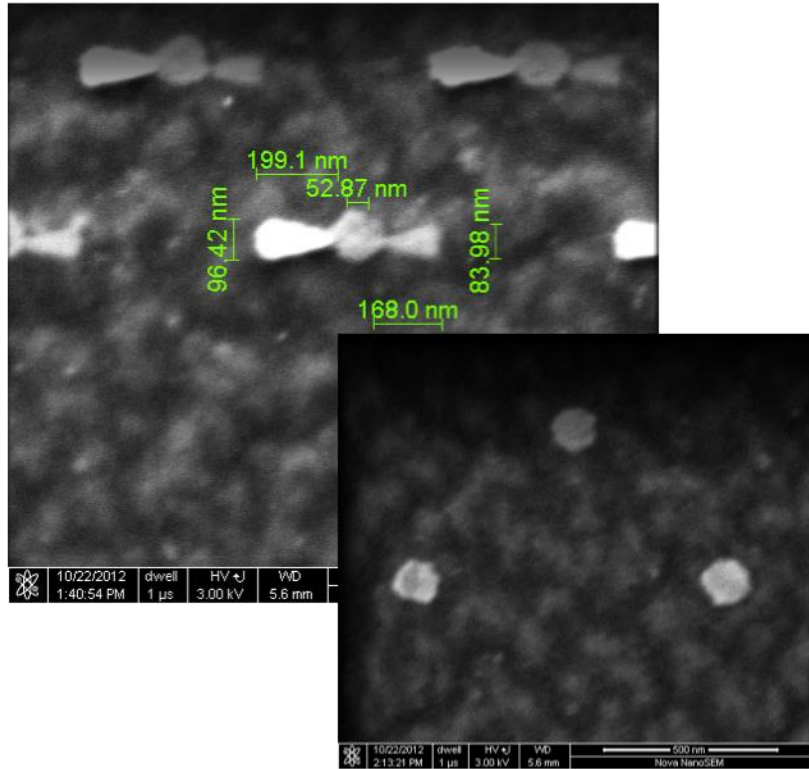


Fig 3.5 Top and Side schematics of the device as well as SEMS

## Chapter 4: Experimental Results and Discussion

Coupling an emitter to an antenna serves two major purposes. Firstly, it speeds up the rate of spontaneous emission as discussed previously. And secondly, it increases the efficiency by increasing the radiative rate with respect to the non-radiative rate. Recalling section 2.4.5, the following expressions show both of these effects:

$$\frac{dN}{dt} = -\frac{N}{\tau(N)} = -(BFN^2 + AN + CN^3) \quad (4.1)$$

$$\eta_r(N) = L_{\text{extraction}} \frac{FDR_{sp}}{FDR_{sp} + R_{nr} + R_{leakage}} \quad (4.2)$$

where F is the enhancement factor due to the antenna. Both of these consequences can be experimentally tested to measure the enhancement factor with caveats. In this work, we concentrate on measuring the second factor due to the reasons below

The rate of recombination in a semiconductor can be measured by pulsing the material with a femtosecond laser and monitoring the photon emission as a function of time. It is important to note that the photon decay rate determines the recombination rate of all mechanisms – radiative as well as non-radiative since the emission is dependent on the carrier concentration seen in eq 4.1. Thus, a faster decay rate can be achieved both by an antenna/cavity effect or by a greater non-radiative component. Additionally measurable decay times in the NIR with fast photodetectors, streak cameras or APDs are in the picosecond regime, already on the border or too slow to measure the recombination times and we expect to see. Additionally equipment this fast generally commands a hefty price tag and can be less sensitive than necessary for this application. Future work with this technique will be discussed in chapter 5.

The relative efficiency on the other hand can be measured by the relative increase in light output. While non-radiative recombination may increase with the addition of an antenna, an increase in efficiency will mean a relatively greater enhancement factor, placing a lower bound on the enhancement. Analyzing the spectrum also confirms the resonant nature of the antenna. However, an increase in light output through other mechanisms, normally a bonus, can obfuscate the determination of the enhancement factor. An increased injection of carriers when optically pumping, light trapping/extraction enhancement by the non-planar surface (denoted  $L_{\text{extraction}}$  in eq 4.2), and increased output from directivity of the antenna(D in eq 4.2) all increase the light output. The directivity was discussed in chapter 2.2.4 and light tapping/extraction and resonant pumping will be discussed in the following sections.

The basic experimental setup is a laser impinging upon the antenna array. The collected light is then input into a spectrometer and passed to a liquid nitrogen cooled InGaAs CCD shown in fig 4.1. To obtain reflection data, a white light replaces the laser.

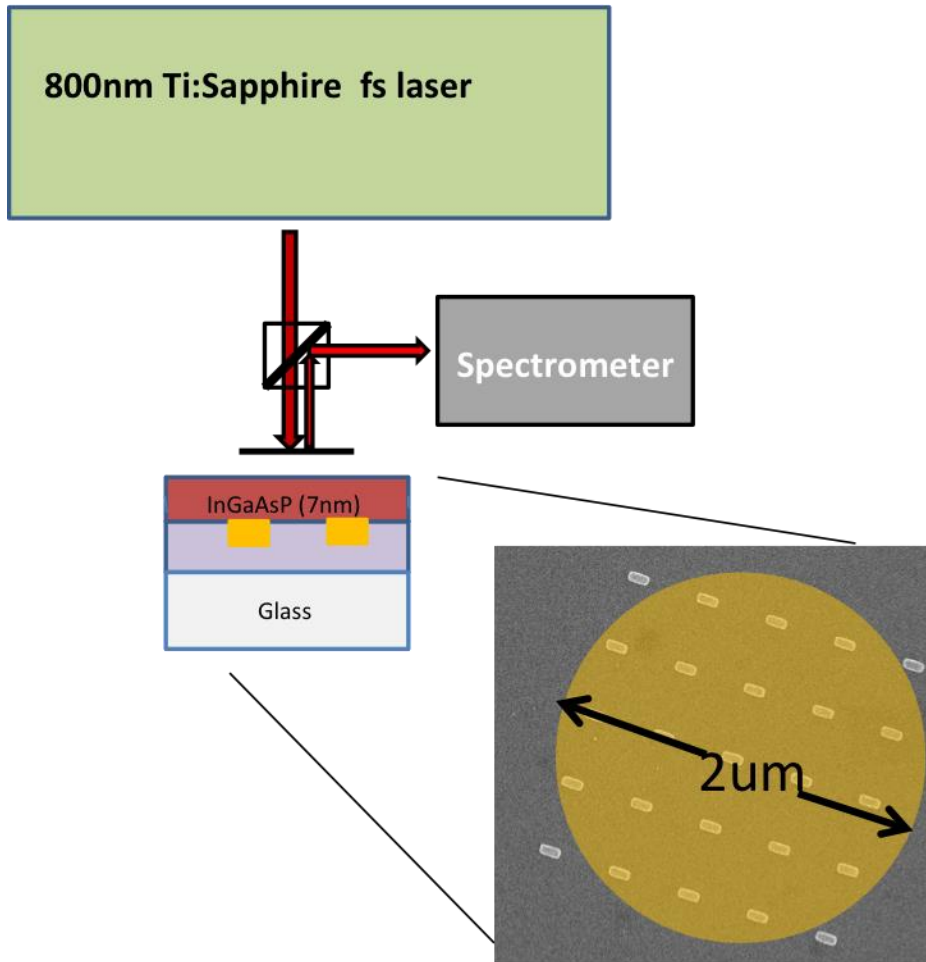


Fig 4.1. Schematic of the experimental setup. A Femtosecond laser is incident on an array of antennas coupled to InGaAsP. The PL is subsequently sent to a spectrometer.

## 4.1 Light trapping and Extraction Enhancement

Initial experiments were performed on a 20nm layer of InGaAsP on top of a 55nm layer of InP to determine the resonance of the antennas. White light polarized parallel to the long axis of the antenna will experience a dip where the resonance is, due to absorption at this frequency and scattering in all directions rather reflection straight up. Laser light pumped perpendicular to the antenna axis to avoid resonant pumping described in the next section, shows enhancement at this frequency shown in fig 4.2.

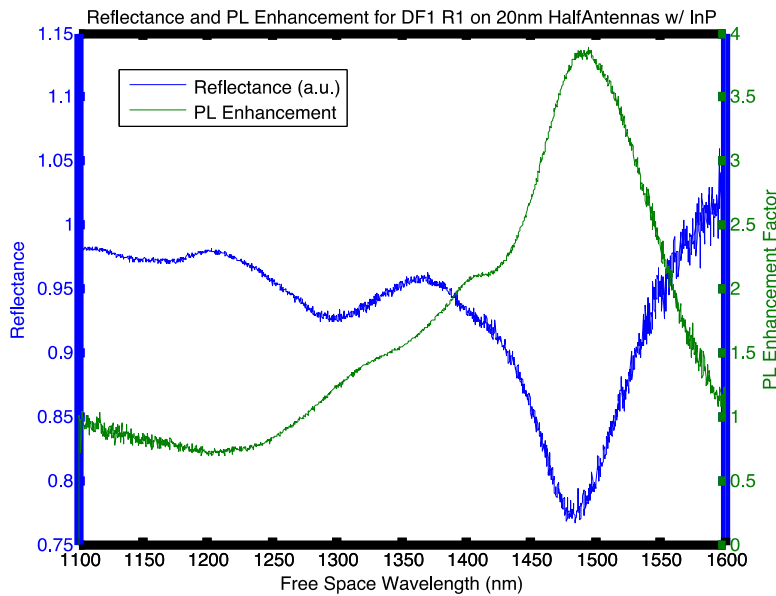


Fig 4.2. Reflectance and PL enhancement from a 160nm metal bar on 20nm InGaAsP/55nm InP

Here we see that the resonance for a gold antenna bar of 160nm in length has a resonance frequency at a free space wavelength of 1480nm. The antenna is shorter than a half wavelength due to the fact that it lies on a half-plane with  $n \sim 3.5$ . If we take the resonance frequency  $\omega = 1/\sqrt{LC}$ , we notice that the increasing the capacitance by surrounding it dielectric decreases its resonance frequency, thus increasing its resonant wavelength. Additionally the kinetic inductance of the gold bar increases  $L$ , further increasing the resonant wavelength. Similar experiments of this nature have been shown, and naively one may conclude that the enhancement is simply 4 from the graph. While some information may be gained about the resonance frequency and  $Q$  of this antenna, the enhancement factor is clouded by the fact that light can more readily escape through scattering.

A simple example of this is shown in fig 4.3. In the ray optics picture, emission that occurs outside the critical angle gets trapped within the semiconductor. When the surface is roughened the angle of emission is randomized and far more light can escape since it is not trapped. Similarly, a plane wave incidence will yield a higher absorption in the textured semiconductor. The light that would normally pass through or be reflected can potentially scatter back into the semiconductor and thus the path length of the photon increases.

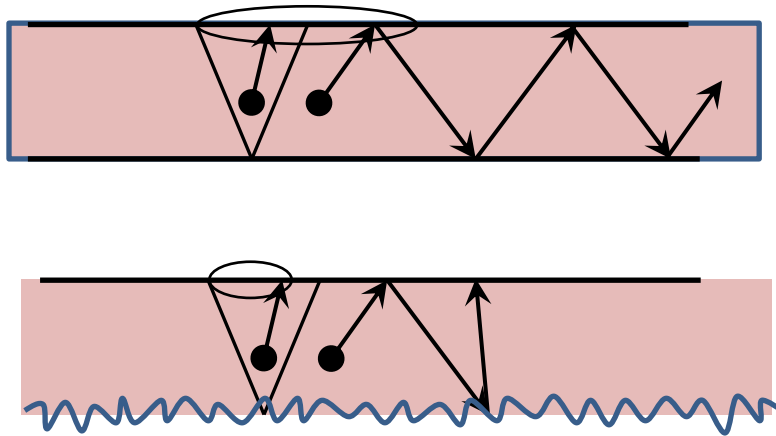


Fig 4.3 Schematic of light rays emitted within a material with planar facets (top) and with a roughened facet (bottom)

The two processes both rely upon the same derivation, given by Yablonovitch in 1982, and the enhancements are equivalent to  $4n^2 \sim 50x$  where  $n$  is the refractive index [31]. A simple random texture can both boost the absorption and emission by a thin semiconductor layer, an engineering trick that is now being employed in both solar cells as well as LEDs. In the case of a structure depicted in fig 4.2, the structure is sub-wavelength and the ray optics picture does not apply. The semiconductor layer does not support a transverse mode due to its asymmetry; however, it can support a leaky mode which can be partially guided before curving into the epoxy beneath it. Scattering centers thus will still boost the extraction efficiency but not nearly to the extent of the  $4n^2$  that occurs in the ray optics regime.

Thus, to avoid enhanced absorption and extraction the excess semiconductor must be etched away, preventing any waveguiding. This provides the added benefit of measuring the PL of the InGaAsP that couples best to the antenna.

## 4.2 Resonant Pump Enhancement

Since antennas are reciprocal devices, pumping with the electric field polarization along the antenna's long axis enhances the intensity at the gap or at the ends of the antenna. And since the absorption in the material is dependent upon the intensity, this generates more carriers leading to an increase in photoluminescence. While this does increase the rate, it does so by increased carrier injection, akin to supplying more current in an electrically pumped device, and should not be factored into the spontaneous emission rate enhancement due to the antenna. Even with the pump wavelength detuned from the antenna resonance ( $\sim 800\text{nm}$  vs  $1325\text{nm}$  as in fig 4.4), there can be non-negligible increase in pumping at the edges of the metal.

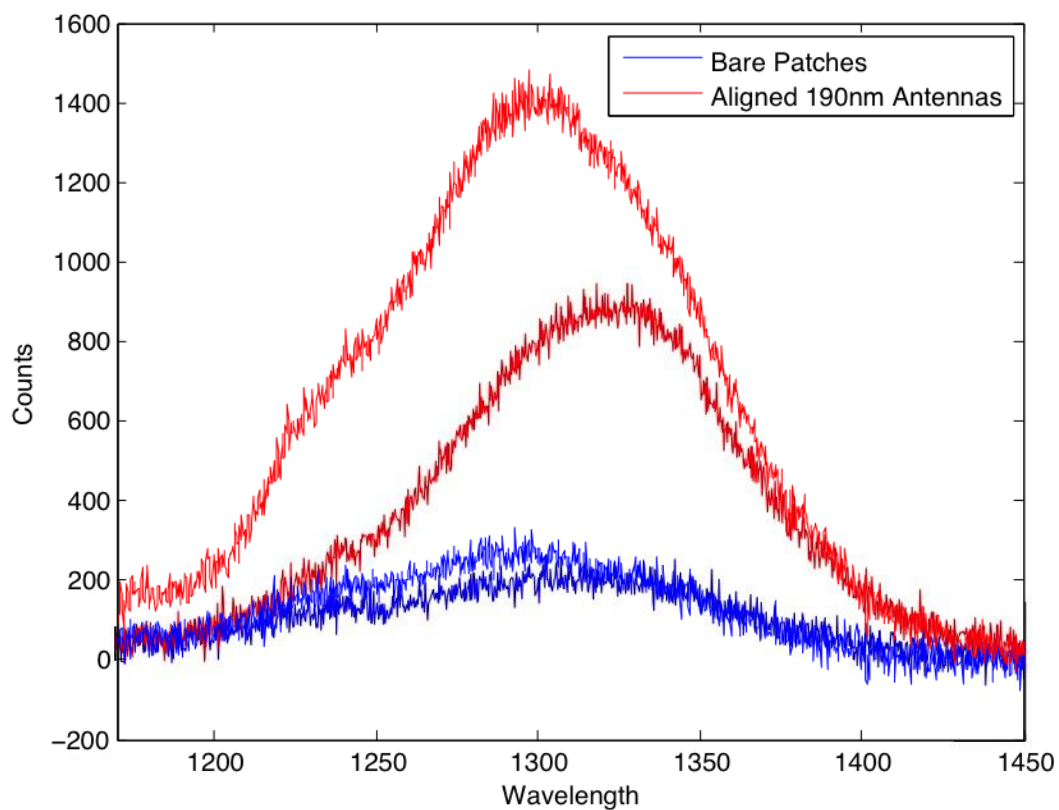


Fig 4.4. Spectrum of PL pumping parallel to the antenna (light red and light blue) vs pumping perpendicular to the antenna (dark red and dark blue). While the emission perpendicular to the antenna is relatively unchanged for both pumping polarizations, the emission in the parallel polarization is enhanced when pumped parallel to the antenna.

For the parallel polarization the emission is much greater due to increased pumping. The peak is roughly 1.5x greater than the perpendicularly pumped antenna and the spectrum is shifted to higher frequencies indicating bandfilling. Resonant pumping of optical antennas can be useful to increase absorption in solar cells, photodetectors and most notably SERS in which the signal receives a pump enhancement as well an emission enhancement. For the case of determining high rate enhancements though, we still restrict ourselves to pumping in the perpendicular polarization.

### 4.3 Bar Antenna Results

Bar antennas were fabricated as detailed in section 3.1 in sizes of 180nm, 200nm and 220nm on patches of diameter 220nm and 350nm. Additionally, bare patches and intentionally misaligned antennas spaced a half period away from the patches are used for control. A Ti:sapphire laser (Coherent chameleon) femtosecond laser pulsed at 80Mhz is pulse picked to a rep rate of 10Mhz is used to pump the arrays as it provides high peak power and minimizes heating of the 7nm

quantum well patches and antennas. It is fed into a short-pass dichroic beamsplitter, passing the 800nm light that is focused to a  $\sim 2\mu\text{m}$  spot size on the sample with a .7 NA objective. The spontaneous emission spectra is then collected via the same objective and reflected by the dichroic into a Princeton Instruments spectrometer diffracted onto a liquid nitrogen cooled InGaAs CCD at  $-110\text{C}$ . The results on the 220nm patch are shown in fig 4.5

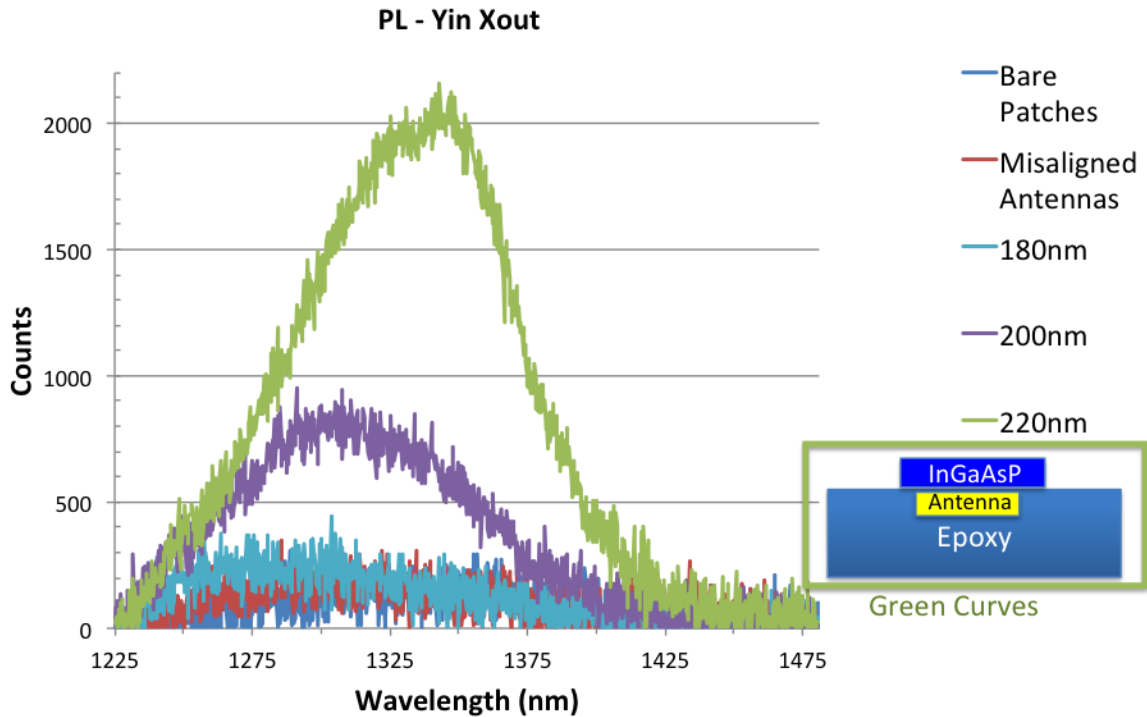


Fig 4.5. Spontaneous emission spectra of singled sided Au antennas of length 180nm, 200nm, 220nm under a InGaAsP cylindrical patch of thickness 7nm and diameter 220nm. Arrays  $10\mu\text{m} \times 10\mu\text{m}$  with an 800nm period are illuminated with a 800nm femtosecond laser polarized perpendicular to the long axis of the antenna and measured parallel. Bare patches and misaligned antennas (by a half period) are shown for comparison.

The results show an enhancement in PL, corresponding to an enhancement in rate. The 220nm long antenna resonance frequency is matched to the spontaneous emission frequency showing a 12.5x enhancement. The 180nm and 200nm long antennas are too short resulting and not on resonance, enhancing only the tail of the PL. And the PL from the misaligned antenna is roughly equivalent to the bare patch indicating that simple scattering of light is not occurring. As the InGaAsP, suffers considerable non-radiative recombination the lifetime is roughly estimated to be  $\sim 50\text{ps}$  for the unenhanced rate and  $\sim 5\text{ps}$  for the enhanced rate. This is determined by assuming a nominal spontaneous lifetime of  $\sim 1\text{ns}$  and measuring 250x reduction in PL from a cladded InGaAsP in InP to a naked InGaAsP layer accounting for the change in absorption. The

reduction can be attributed to a  $\sim 10x$  reduction in absorption length and a  $25x$  reduction in PL due to surface recombination.

Comparing this to the PL measured perpendicular to the antenna we can get an idea of how the metal is affecting the patch in fig.4.6.

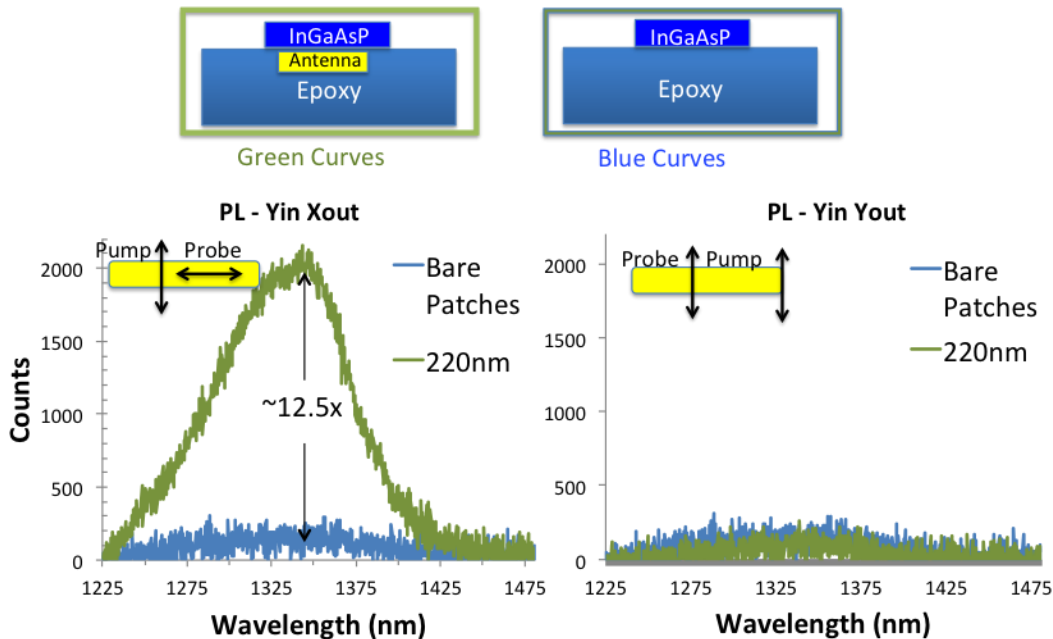


Fig 4.6. Spontaneous emission spectra polarization comparison on the 220nm patches – Emission parallel with the antenna (left) and perpendicular (right)

The polarization dependence of the output light, the resonance shifts dependent on antenna length and the equivalence of the misaligned antenna and bare patch confirm that this is indeed an antenna effect. The perpendicularly polarized light is slightly lower than the bare patches indicating that if there is an enhancement in absorption due to the off-resonance/off-polarized laser light, it is offset by non-radiative recombination due to the metal contact. Since the non-radiative terms dominate, the PL enhancement is roughly equivalent to the rate enhancement.

The 350nm patches (fig 4.7) show similar results with a lower enhancement. The near field of an antenna falls off very quickly and so only the closest dipole couple well. Therefore, to a rough approximation we can assume the excess InGaAsP surrounding the 220nm patch adds only to the background signal. Only  $\sim 40\%$  of the area is coupled well enough to the antenna to obtain a  $12.5x$  enhancement yielding an expected enhancement of  $4.9x$  for the 350nm patch, in good agreement with the measured results.

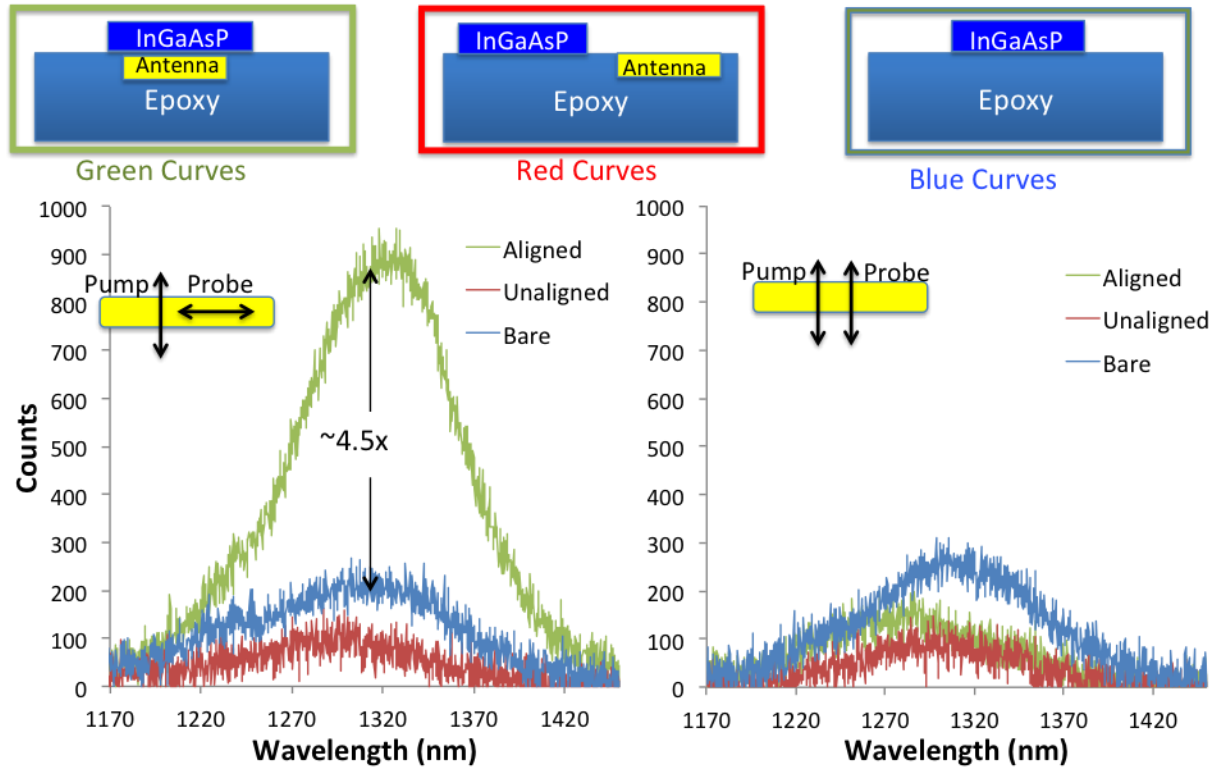


Fig 4.7 Spontaneous emission spectra polarization comparison on the 350nm patches – Emission parallel with the antenna (left) and perpendicular (right)

#### 4.4 Bowtie Antenna results

Our bowtie antennas were fabricated upon 125nm InGaAsP patches with the process outlined in chapter 3. Our detector could not resolve the PL from bare patches or signals from antennas measuring the perpendicularly polarized light. Nevertheless some interesting observations can be made. Fig 4.8 shows the PL spectrum of a bowtie antenna pumped with perpendicularly polarized light and measured parallel compared to pumping a patch. The spectrum shows an enhancement of ~20x compared to the noise floor. Rather than measuring a spectrum, the light can be focused down to one pixel, allowing for a better signal to noise ratio. Doing so gives us the plots shown in fig 4.9 in which the best antennas out of each alignment are pumped with perpendicularly polarized light and measured with light polarized parallel to the antenna (shown in blue) and light polarized perpendicular to the antenna. While the alignments can deviate slightly, the general trend is unambiguous. The longer the antenna is compared to the gap, the greater the radiation resistance according to our formula initially shown in chapter 2:

$$\frac{1/\tau_{ant}}{1/\tau_{dipole}} = \frac{1}{4} \left( \frac{l}{d} \right)^2$$

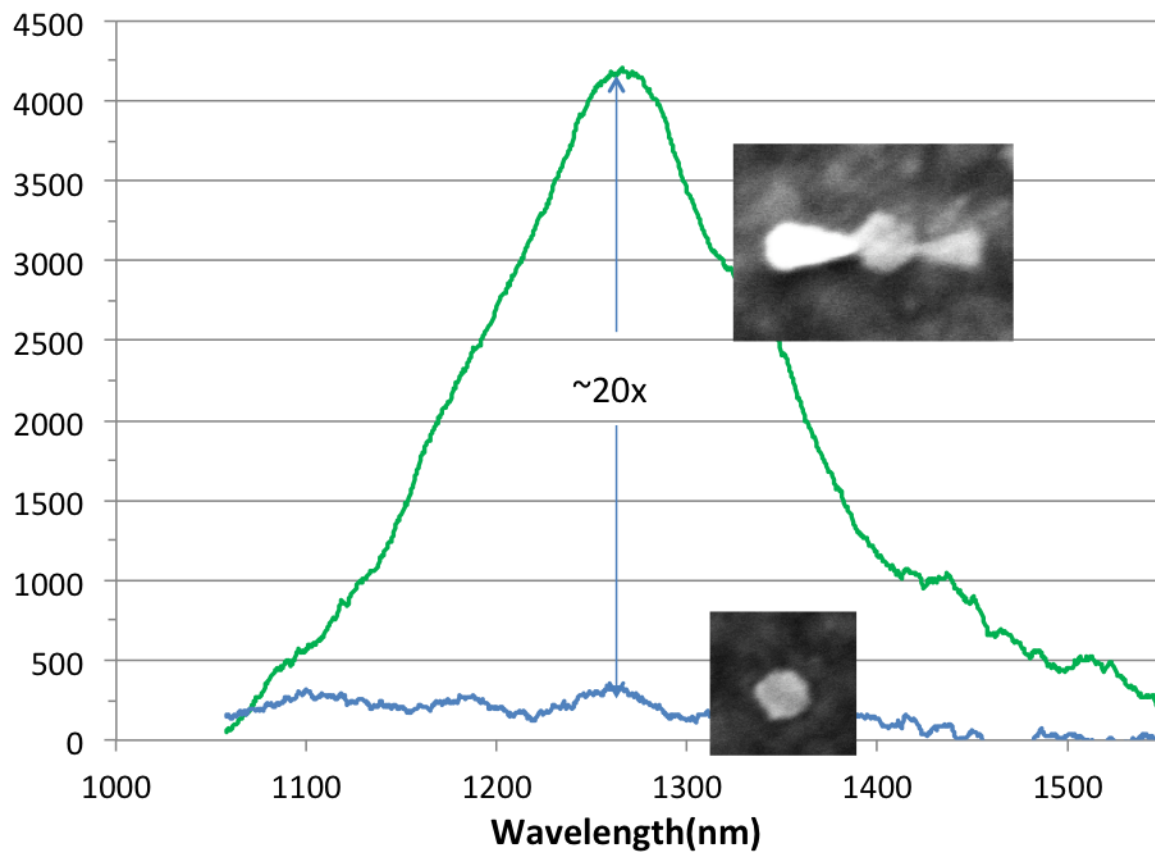


Fig 4.8 Spectrum from PL(in the antenna polarization) from an antenna with half-length 200nm vs a bare patch of InGaAsP.

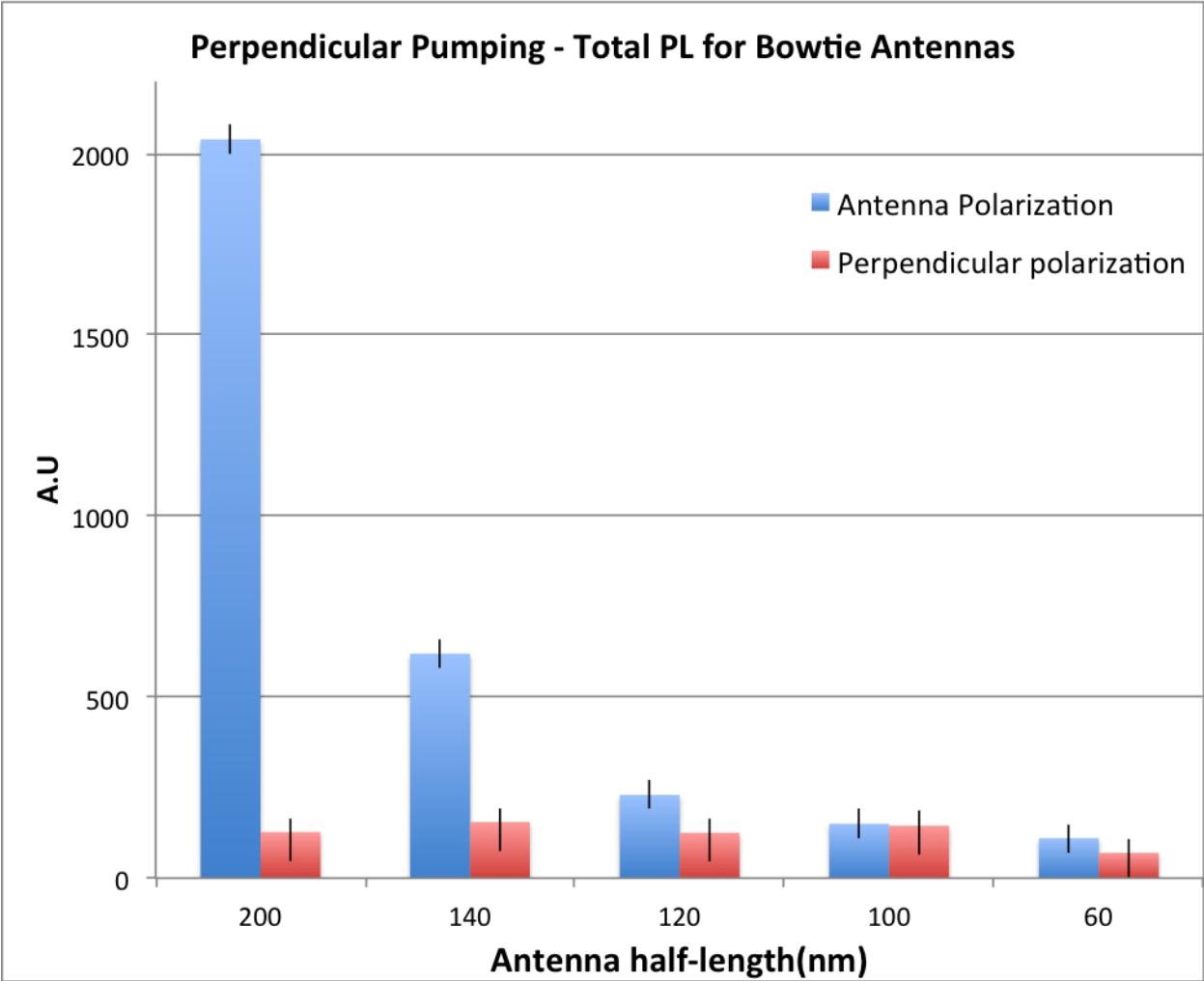


Fig 4.9 PL from various antenna sizes in the antenna polarization(blue) and the perpendicular polarization (red). The perpendicular polarization was used to pump the antennas.

Since the signal is buried in the noise for a patch, we can compare the best 200nm antenna to the best 60nm, which will give a lower bound on the enhancement. Doing so gives us fig 4.10:

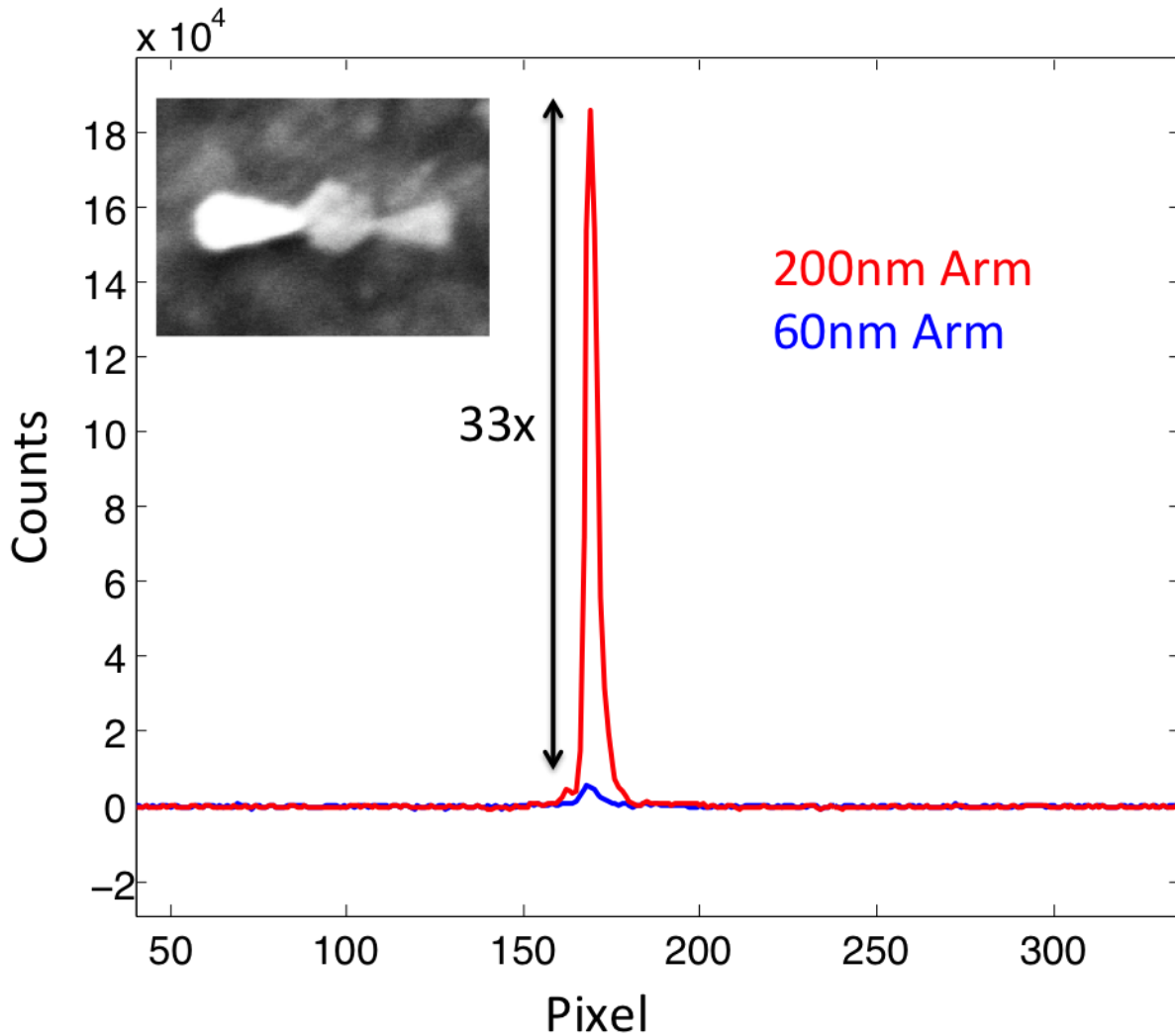


Fig 4.10 Total PL (in the antenna polarization) from an antenna with half-length of 200nm vs a half-length of 60nm.

These enhancement factors are quite large, but not as large as we expect to see given the theory in chapter 2. It is also difficult to accurately measure the gap size due to misalignment. One consideration we have not touched upon yet is the diffusion of carriers. In this work we did not explicitly seek to improve surface recombination through passivation or other means and thus the diffusion length of carriers given by  $L_{\text{Diff}} = (D\tau)^{1/2}$  can be quite high. Using the nominal rate that we expect from before,  $L_{\text{diff}}$  can be on the order of 20nm. Pumping therefore produces carriers that non-radiatively recombine before they can diffuse to the hot spots of the antenna, weakening the overall enhancement. The quantum well being only 7nm thick makes surface recombination a serious problem. Additionally, gold is directly in contact with the semiconductor in order to provide the smallest gaps possible for the greatest enhancements. As seen in fig 4.11 taken from[32], metals such as gold and silver greatly increase surface recombination velocity in InP and is expected to do the same for similar materials.

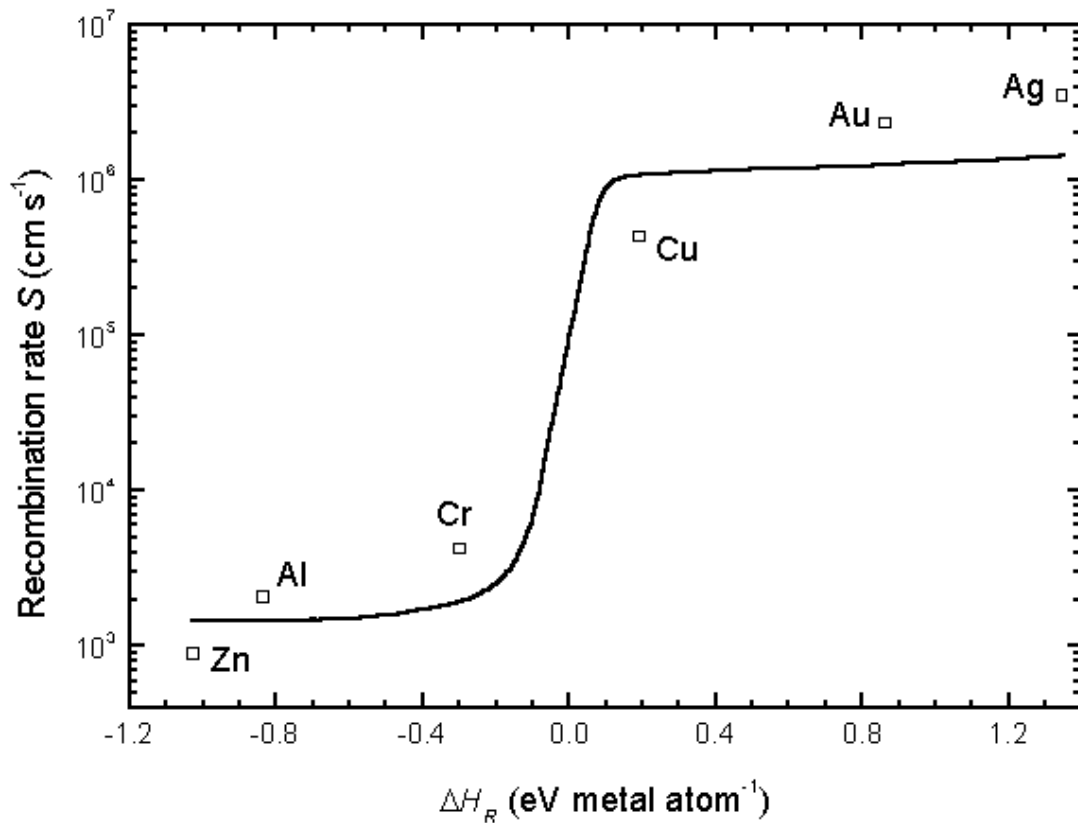


Fig 4.11 The recombination rate as plotted as a function of heat of reaction per metal atom. Data points for specific metals are plotted[32].

Therefore, future optical antennas of this nature should be passivated. Options typically involve an ammonium hydroxide dip to remove oxidized states, followed by various surface treatments including sulfur treatments [33]. Wet chemical passivation tends to last only a short while in atmosphere so capping layers of oxides or nitrides are a possibility[34]. A more practical use of optical antennas, when coupled to a waveguide may not suffer from this as much as InP reduces dangling bonds.

## Chapter 5: Future Work and Conclusion

Thus far we have discussed the theory behind optical antennas and the experimental work that showed the proof of principle. Much more can be done in this promising field, and far more needs to be done to make this a viable technology for short distance optical interconnects. Further confirmation of the high enhancements from optical antennas can be done by switching to lower wavelengths where detection by higher sensitivity and faster are more common place. Switching to a material such as InP which already boasts lower surface recombination velocities can greatly increase efficiencies while also making it easier to do time resolved measurements. Passivation can also greatly aid in experimentally verifying higher enhancements by lowering the surface recombination due to the metal.

Electrical injection is also required for practical use in this field. Ideally the antenna itself would be used as an electrode and recent work has shown this may be possible [35] by connecting the leads at regions with lower near field intensities.

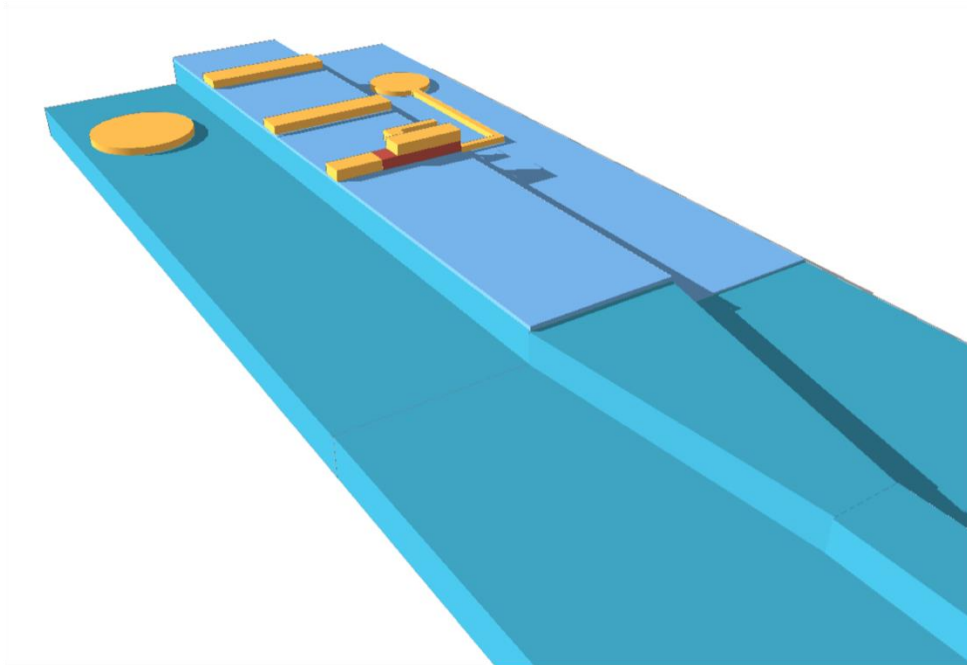


Fig 5.1 Schematic of potential Spontaneous Hyper Emitting Diode.

Finally, the device needs to be coupled to a waveguide. Various antenna concepts such as the Yagi-Uda antenna promote directional propagation and could potentially be used to couple to a waveguide.

In the concept in Fig 5.1, a visual of a potential Spontaneous Hyper Emitting Diode is given. The bottom teal area consists of a n-doped InP waveguide with a ohmic contact for current injection. Atop of the waveguide is a quantum well of InGaAsP coupled to an antenna. The other strips of metal serve as reflectors to direct the beam into the waveguide. The top half of the antenna serves as the p-contact which is isolated from the surrounding material with oxide.

With III-V bonding becoming a viable technique, this process can be transferred to Si for integration with CMOS compatible electronics and silicon waveguides, filters, detectors etc to replace aluminum/copper as communication method of choice.

# Bibliography

- [1] "ITRS 2007 Edition." [Online]. Available: <http://www.itrs.net/Links/2007ITRS/Home2007.htm>. [Accessed: 17-May-2013].
- [2] F. Pollack, "New Microarchitecture Challenges in the Coming Generations of CMOS," 1999.
- [3] D. A. B. Miller, "Optical interconnects to electronic chips," *Appl. Opt.*, vol. 49, no. 25, pp. F59–F70, Sep. 2010.
- [4] S. Perrin, "The need for next-generation roadm networks," *White Paper*, <http://www.heavyreading.com>, 2010.
- [5] M. Nagy, and S. Tibuleac, "Wavelength Selective Switches for Fiber Optic Telecommunications (Photonics Spectra | Nov 2006 | Features)," Nov-2006. [Online]. Available: <http://www.photonics.com/Article.aspx?AID=27188>. [Accessed: 26-Apr-2013].
- [6] E. Marchena, T. Creazzo, S. B. Krasulick, P. Yu, D. Van Orden, J. Y. Spann, C. C. Blivin, J. M. Dallesasse, P. Varangis, R. J. Stone, and A. Mizrahi, "Integrated Tunable CMOS Laser for Si Photonics," 2013, p. PDP5C.7.
- [7] L. Tang, S. E. Kocabas, S. Latif, A. K. Okyay, D.-S. Ly-Gagnon, K. C. Saraswat, and D. A. B. Miller, "Nanometre-scale germanium photodetector enhanced by a near-infrared dipole antenna," *Nature Photonics*, vol. 2, no. 4, pp. 226–229, Mar. 2008.
- [8] H. A. Atwater and A. Polman, "Plasmonics for improved photovoltaic devices," *Nature Materials*, vol. 9, no. 3, pp. 205–213, Feb. 2010.
- [9] Asia-Pacific Workshop on Near Field Optics, *Near-field optics: principles and applications: the second Asia-Pacific Workshop on Near Field Optics, Beijing, China, October 20-23, 1999*. Singapore ; River Edge, N.J.: World Scientific, 2000.
- [10] P. Anger, P. Bharadwaj, and L. Novotny, "Enhancement and Quenching of Single-Molecule Fluorescence," *Physical Review Letters*, vol. 96, no. 11, Mar. 2006.
- [11] S. Kühn, U. Håkanson, L. Rogobete, and V. Sandoghdar, "Enhancement of Single-Molecule Fluorescence Using a Gold Nanoparticle as an Optical Nanoantenna," *Physical Review Letters*, vol. 97, no. 1, Jul. 2006.
- [12] P. Bharadwaj and L. Novotny, "Spectral dependence of single molecule fluorescence enhancement," *Optics Express*, vol. 15, no. 21, p. 14266, 2007.
- [13] W. Zhu, M. G. Banaee, D. Wang, Y. Chu, and K. B. Crozier, "Lithographically fabricated optical antennas with gaps well below 10 nm," *Small*, vol. 7, no. 13, pp. 1761–1766, 2011.
- [14] D. Wang, T. Yang, and K. B. Crozier, "Optical antennas integrated with concentric ring gratings: electric field enhancement and directional radiation," *Opt. Express*, vol. 19, no. 3, pp. 2148–2157, 2011.
- [15] W. A. Challener, C. Peng, A. V. Itagi, D. Karns, W. Peng, Y. Peng, X. Yang, X. Zhu, N. J. Gokemeijer, Y.-T. Hsia, G. Ju, R. E. Rottmayer, M. A. Seigler, and E. C. Gage, "Heat-assisted magnetic recording by a near-field transducer with efficient optical energy transfer," *Nature Photonics*, vol. 3, no. 4, pp. 220–224, Mar. 2009.
- [16] "Letters to the editor," *Antennas and Propagation Magazine, IEEE*, vol. 46, no. 2, pp. 130–131, Apr. 2004.
- [17] "Radio's First Message -- Fessenden and Marconi." [Online]. Available: [http://www.ieee.ca/millennium/radio/radio\\_differences.html](http://www.ieee.ca/millennium/radio/radio_differences.html). [Accessed: 18-Mar-2013].

- [18] C. A. Balanis, "Antenna theory: a review," *Proceedings of the IEEE*, vol. 80, no. 1, pp. 7–23, Jan. 1992.
- [19] W. E. Willshaw, L. Rushforth, A. G. Stainsby, R. Latham, A. W. Balls, and A. H. King, "The high-power pulsed magnetron: development and design for radar applications," *Electrical Engineers - Part IIIA: Radiolocation, Journal of the Institution of*, vol. 93, no. 5, p. 985, 1946.
- [20] "Magnetism, Radiation, and Relativity." [Online]. Available: <http://physics.weber.edu/schroeder/mrr/MRRtalk.html>. [Accessed: 19-Mar-2013].
- [21] H. A. Wheeler, "Fundamental Limitations of Small Antennas," *Proceedings of the IRE*, vol. 35, no. 12, pp. 1479–1484, Dec. 1947.
- [22] T. H. Glisson, *Introduction to Circuit Analysis and Design*. Springer London, Limited, 2010.
- [23] S. A. Maier, *Plasmonics: fundamentals and applications*. New York: Springer, 2007.
- [24] P. B. Johnson and R. W. Christy, "Optical Constants of the Noble Metals," *Physical Review B*, vol. 6, no. 12, pp. 4370–4379, Dec. 1972.
- [25] P. W. Gilberd, "The anomalous skin effect and the optical properties of metals," *Journal of Physics F: Metal Physics*, vol. 12, no. 8, pp. 1845–1860, Aug. 1982.
- [26] L. Novotny, *Principles of nano-optics*. Cambridge ; New York: Cambridge University Press, 2006.
- [27] "Proceedings of the American Physical Society," *Physical Review*, vol. 69, no. 11–12, pp. 674–674, Jun. 1946.
- [28] E. K. Lau, A. Lakhani, R. S. Tucker, and M. C. Wu, "Enhanced modulation bandwidth of nanocavity light emitting devices," *Optics Express*, vol. 17, no. 10, p. 7790, Apr. 2009.
- [29] W. Shockley, "Currents to Conductors Induced by a Moving Point Charge," *Journal of Applied Physics*, vol. 9, no. 10, p. 635, 1938.
- [30] S. Ramo, "Currents Induced by Electron Motion," *Proceedings of the IRE*, vol. 27, no. 9, pp. 584–585, Sep. 1939.
- [31] E. Yablonovitch, "Statistical ray optics," *Journal of the Optical Society of America*, vol. 72, no. 7, p. 899, Jul. 1982.
- [32] Y. Rosenwaks, Y. Shapira, and D. Huppert, "Metal reactivity effects on the surface recombination velocity at InP interfaces," *Applied Physics Letters*, vol. 57, no. 24, p. 2552, 1990.
- [33] Z. Jin, S. Neumann, W. Prost, and F.-J. Tegude, "Effects of (NH<sub>4</sub>)<sub>2</sub>S passivation on the performance of graded-base InGaAs/InP HBTs," *physica status solidi (a)*, vol. 201, no. 5, pp. 1017–1021, Apr. 2004.
- [34] Z. Jin, W. Prost, S. Neumann, and F.-J. Tegude, "Comparison of the passivation effects on self- and non-self-aligned InP/InGaAs/InP double heterostructure bipolar transistors by low-temperature deposited SiN<sub>x</sub>," *Journal of Applied Physics*, vol. 96, no. 1, p. 777, 2004.
- [35] J. C. Prangma, J. Kern, A. G. Knapp, S. Grossmann, M. Emmerling, M. Kamp, and B. Hecht, "Electrically Connected Resonant Optical Antennas," *Nano Letters*, vol. 12, no. 8, pp. 3915–3919, Aug. 2012.
- [36] A. Kinkhabwala, Z. Yu, S. Fan, Y. Avlasevich, K. Müllen, and W. E. Moerner, "Large single-molecule fluorescence enhancements produced by a bowtie nanoantenna," *Nature Photonics*, vol. 3, no. 11, pp. 654–657, Oct. 2009.

- [37] O. L. Muskens, V. Giannini, J. A. Sánchez-Gil, and J. Gómez Rivas, "Strong Enhancement of the Radiative Decay Rate of Emitters by Single Plasmonic Nanoantennas," *Nano Letters*, vol. 7, no. 9, pp. 2871–2875, Sep. 2007.
- [38] J. R. Lakowicz and Y. Fu, "Modification of single molecule fluorescence near metallic nanostructures," *Laser & Photonics Review*, vol. 3, no. 1–2, pp. 221–232, Feb. 2009.
- [39] R. M. Bakker, H.-K. Yuan, Z. Liu, V. P. Drachev, A. V. Kildishev, V. M. Shalaev, R. H. Pedersen, S. Gresillon, and A. Boltasseva, "Enhanced localized fluorescence in plasmonic nanoantennae," *Applied Physics Letters*, vol. 92, no. 4, p. 043101, 2008.
- [40] D. V. Guzатов, S. V. Vaschenko, V. V. Stankevich, A. Y. Lunevich, Y. F. Glukhov, and S. V. Gaponenko, "Plasmonic Enhancement of Molecular Fluorescence near Silver Nanoparticles: Theory, Modeling, and Experiment," *The Journal of Physical Chemistry C*, vol. 116, no. 19, pp. 10723–10733, May 2012.
- [41] I. Kocakarın and K. Yegin, "Surface Plasmon-Enhanced Nanoantenna for Localized Fluorescence," *International Journal of Antennas and Propagation*, vol. 2012, pp. 1–7, 2012.
- [42] Y. Zhao, N. Engheta, and A. Alù, "Effects of shape and loading of optical nanoantennas on their sensitivity and radiation properties," *Journal of the Optical Society of America B*, vol. 28, no. 5, p. 1266, Apr. 2011.
- [43] X. Gu, T. Qiu, W. Zhang, and P. K. Chu, "Light-emitting diodes enhanced by localized surface plasmon resonance," *Nanoscale Research Letters*, vol. 6, no. 1, p. 199, 2011.
- [44] S. V. Boriskina and L. Dal Negro, "Multiple-wavelength plasmonic nanoantennas," *Optics Letters*, vol. 35, no. 4, p. 538, Feb. 2010.
- [45] T. Kosako, Y. Kadoya, and H. F. Hofmann, "Directional control of light by a nano-optical Yagi–Uda antenna," *Nature Photonics*, vol. 4, no. 5, pp. 312–315, Mar. 2010.
- [46] Y. Fu, J. Zhang, and J. R. Lakowicz, "Plasmon-Enhanced Fluorescence from Single Fluorophores End-Linked to Gold Nanorods," *Journal of the American Chemical Society*, vol. 132, no. 16, pp. 5540–5541, Apr. 2010.
- [47] J. N. Farahani, D. W. Pohl, H.-J. Eisler, and B. Hecht, "Single Quantum Dot Coupled to a Scanning Optical Antenna: A Tunable Superemitter," *Physical Review Letters*, vol. 95, no. 1, Jun. 2005.
- [48] K. C. Y. Huang, M.-K. Seo, Y. Huo, T. Sarmiento, J. S. Harris, and M. L. Brongersma, "Antenna electrodes for controlling electroluminescence," *Nature Communications*, vol. 3, p. 1005, Aug. 2012.
- [49] T. Feichtner, O. Selig, M. Kiunke, and B. Hecht, "Evolutionary Optimization of Optical Antennas," *Physical Review Letters*, vol. 109, no. 12, Sep. 2012.
- [50] M. Eggleston, A. Lakhani, L. Zhang, E. Yablonovitch, and M. C. Wu, "<![CDATA[Optical antenna based nanoLED]]>," 2011, pp. 177–178.
- [51] M. Eggleston, N. Kumar, K. Messer, L. Zhang, E. Yablonovitch, and M. C. Wu, "Efficient Rate Enhancement of Spontaneous Emission in a Semiconductor nanoLED," 2012, p. FW6C.8.
- [52] G. Shambat, B. Ellis, A. Majumdar, J. Petykiewicz, M. A. Mayer, T. Sarmiento, J. Harris, E. E. Haller, and J. Vučković, "Ultrafast direct modulation of a single-mode photonic crystal nanocavity light-emitting diode," *Nature Communications*, vol. 2, p. 539, Nov. 2011.

- [53] N. R. Kumar, K. Messer, M. Eggleston, M. C. Wu, and E. Yablonovitch, “Spontaneous emission rate enhancement using gold nanorods,” 2012, pp. 612–613.
- [54] C. Farcău and S. Aștilean, “Silver half-shell arrays with controlled plasmonic response for fluorescence enhancement optimization,” *Applied Physics Letters*, vol. 95, no. 19, p. 193110, 2009.
- [55] G. Vecchi, V. Giannini, and J. Gómez Rivas, “Shaping the Fluorescent Emission by Lattice Resonances in Plasmonic Crystals of Nanoantennas,” *Physical Review Letters*, vol. 102, no. 14, Apr. 2009.
- [56] Q.-H. Park, “Optical antennas and plasmonics,” *Contemporary Physics*, vol. 50, no. 2, pp. 407–423, Mar. 2009.
- [57] A. Mohammadi, V. Sandoghdar, and M. Agio, “Gold nanorods and nanospheroids for enhancing spontaneous emission,” *New Journal of Physics*, vol. 10, no. 10, p. 105015, Oct. 2008.

# Appendix 1: Derivation of Fields from a Hertzian Dipole

Consider a conductor (with no net charge) along the z axis of length L with an oscillating current  $I_0$ .

$$I = I_0 \cos(\omega t)$$

The magnetic vector potential is given by:

$$\mathbf{A}(\mathbf{r}, t) = \frac{\mu_0}{4\pi} \int \frac{\mathbf{j}\left(\mathbf{r}', t - \frac{|\mathbf{r} - \mathbf{r}'|}{c}\right)}{|\mathbf{r} - \mathbf{r}'|} dV'$$

For a conductor of negligible thickness we can replace  $\mathbf{j}$  with  $I dz$  and so,

$$\mathbf{A}(\mathbf{r}, t) = \frac{\mu_0}{4\pi} \int \frac{I\left(z', t - \frac{|\mathbf{r} - z'\hat{\mathbf{z}}|}{c}\right)}{|\mathbf{r} - z'\hat{\mathbf{z}}|} dz'$$

In the region  $r \gg L$

$$|\mathbf{r} - z'\hat{\mathbf{z}}| \approx r$$

and so the equation simplifies to:

$$A_z(\mathbf{r}, t) = \frac{\mu_0}{4\pi} \int \frac{I\left(z', t - \frac{r}{c}\right)}{r} dz'$$

which is simply

$$A_z(\mathbf{r}, t) = \frac{\mu_0 L}{4\pi} \frac{I\left(t - \frac{r}{c}\right)}{r}$$

To calculate the Electric field from this we must first calculate the potential using the Lorenz gauge:

$$\nabla \cdot \mathbf{A} = -\epsilon_0 \mu_0 \frac{\partial \phi}{\partial t}$$

Solving for  $\phi$ , we obtain:

$$\phi = \frac{L}{4\pi\epsilon_0 c r} \frac{z I\left(t - \frac{r}{c}\right)}{r}$$

The electric field is then given by:

$$\mathbf{E} = -\frac{\partial \mathbf{A}}{\partial t} - \nabla \phi$$

which after some algebra and switching to polar coordinates equates to:

$$\mathbf{E}(r, \theta) = -\frac{\frac{\omega L I_0}{4\pi \epsilon_0 c^2} \sin \theta \sin\left(\omega\left(t - \frac{r}{c}\right)\right)}{r} \hat{\theta}$$

Note that this varies as  $r^{-1}$  in the far field and is completely symmetric about the azimuthal angle  $\phi$ . As discussed in chapter 1, we see that there is no radiation for  $\theta = 0$ .

The total power radiated is given by the Poynting vector integrated over the surface. Since the flux will vary as  $r^{-2}$  any surface chosen will do.

$\mathbf{B}$  is given by:

$$\mathbf{B} = \nabla \times \mathbf{A}$$

And the total power radiated is equivalent to:

$$P = \oint \mathbf{E} \times \frac{\mathbf{B}}{\mu_0} \cdot d\mathbf{S}$$

Integrating gives us the following which is equivalent to the method derived in Chapter 2.

$$P = \frac{q^2 L^2 \omega^4}{12\pi \epsilon_0 c^3}$$

## Appendix 2: Methods for deriving spontaneous emission.

Using thermodynamics, Einstein initially predicted stimulated emission and its relation to absorption and spontaneous emission and his derivation is given here. Let  $N_1$  and  $N_2$  be the number of electrons in the energy levels  $E_1$  and  $E_2$ , in an atom. The rate at which  $N_1$  changes due to the absorption of radiation, with the atom making an upward transition to level  $E_2$ , is assumed to be proportional to  $N_1$  and the spectral energy density  $\rho(\omega_o)$  at its transition frequency  $\omega_o = (E_2 - E_1)/\hbar$ :

$$(\dot{N}_1)_{abs} = B_{12}N_1\rho(\omega_o)$$

Einstein proposes two kinds of emission processes by which an atom can jump from level  $E_2$  to  $E_1$  with the emission of radiation of frequency  $\omega_o$ . One is spontaneous emission, which can occur in the absence of any radiation and is described by the rate constant  $A_{21}$ :

$$(\dot{N}_1)_{spontaneous\ emission} = A_{21}N_2$$

The other is stimulated emission, which is assumed to proceed at a rate proportional to both  $N_2$  and  $\rho(\omega_o)$ :

$$(\dot{N}_1)_{stimulated\ emission} = B_{21}N_2\rho(\omega_o)$$

The condition for equilibrium is

$$(\dot{N}_1)_{absorption} + (\dot{N}_1)_{spontaneous\ emission} + (\dot{N}_1)_{stimulated\ emission} = 0$$

or

$$A_{21}N_2 + B_{21}N_2\rho(\omega_o) = B_{12}N_1\rho(\omega_o)$$

$$\rho(\omega_o) = \frac{A_{21}/B_{21}}{(B_{12}/B_{21})(N_1/N_2) - 1} = \frac{A_{21}/B_{21}}{(B_{12}/B_{21})e^{\hbar\omega_o/kT} - 1}$$

since  $(N_1/N_2) = e^{-(E_2-E_1)/kT} = e^{\hbar\omega_o/kT}$  in thermal equilibrium. At very high temperatures  $\rho(\omega_o)$  becomes so large that spontaneous emission is much less probable than stimulated emission. Then from (4.5) we must have  $B_{21} = B_{12}$ , and from (4.6),

$$\rho(\omega_o) = \frac{A_{21}/B_{21}}{e^{\hbar\omega_o/kT} - 1}$$

For  $kT \gg \hbar\omega_o$ , furthermore,

$$\rho(\omega_o) \cong \frac{A_{21}}{B_{21}} \frac{kT}{\hbar\omega_o}$$

This is the limit where the radiation energy quanta are so small compared with  $kT$  that the classical Rayleigh-Jeans law should be applicable. Comparing Eqn. (4.8) to Eqn. (3.2) we see that this requires  $(A_{21}/B_{21})(kT/\hbar\omega_0) = (\omega_0^2/\pi^2c^3)kT$ , or

$$\frac{A_{21}}{B_{21}} = \frac{\hbar\omega_0^3}{2\pi^2c^3}$$

and Eqn. (4.6) then yields the Planck spectrum for  $\rho(\omega)$ .

## Method I: Detailed Balancing

Imagine a two-level system and consider an electric field with magnitude  $E_p \cos(\omega t)$  where  $E_p$  denotes the peak electric field. By definition then the root mean square electric field is

$$E_{rms} = \sqrt{\langle E_p^2 \cos^2(\omega t) \rangle} = E_p/\sqrt{2}$$

$$E_{rms}^2 = E_p^2/2,$$

and the root mean square energy density of the vacuum field (in  $J/m^3$ ) ignoring dispersion is

$$\frac{\epsilon_0}{2} E_{rms}^2 + \frac{1}{2\mu_0} B_{rms}^2.$$

But, from Faraday's law, assuming a plane wave solution with field dependence  $\propto e^{i(kr-\omega t)}$

$$\nabla \times E = -\frac{\partial B}{\partial t}$$

$$ikE = i\omega B$$

$$\omega^2 B^2 = k^2 E^2$$

$$\frac{B^2}{\mu_0} = \frac{k^2}{\mu_0 \omega^2} E^2 = \frac{\omega^2}{\mu_0 \omega^2 c} E^2 = \epsilon_0 E^2$$

$$\frac{\epsilon_0}{2} E_{rms}^2 + \frac{1}{2\mu_0} B_{rms}^2 = \epsilon_0 E_{rms}^2$$

or, in some material  $= n^2 \epsilon_0 E_{rms}^2$  ( $J/m^3$ ) which is just a statement that in general the electric and magnetic energy densities are equal. The power flux is then

$$\text{Group velocity (m/s)} \times \text{Energy density (J/m}^3) \rightarrow \text{Power flux (W/m}^2).$$

Ignoring dispersion, the group velocity is the same as the phase velocity  $c/n$ , so we have

$$\text{Power flux} = \frac{c}{n} \times n^2 \epsilon_0 E_{rms}^2 = cn \epsilon_0 E_{rms}^2 \text{ (W/m}^2\text{)}.$$

The rate of absorption of energy by a two-level system is simply

$$\alpha \cdot cn \epsilon_0 E_{rms}^2 \text{ (J/s)}$$

where  $\alpha$  is the absorption coefficient and has units of  $m^2$ . Equating the absorption rate to the transition rate from Fermi's golden rule implies that at equilibrium

$$\alpha \cdot cn \epsilon_0 E_{rms}^2 = \frac{2\pi}{\hbar} \hbar \omega |\langle qx E_{p,x}/2 \rangle|^2 \frac{dN}{dE}$$

but

$$|\langle E_{p,x}/2 \rangle|^2 = \frac{E_{p,x}^2}{4} = \frac{1}{2} \cdot \frac{E_{p,x}^2}{2} = \frac{E_{rms,x}^2}{2},$$

where here we only consider the  $x$ -component of polarization

$$E_{rms,x}^2 = \frac{1}{3} \langle E_x^2 + E_y^2 + E_z^2 \rangle = \frac{1}{3} E_{rms}^2$$

$$\alpha \cdot cn \epsilon_0 E_{rms}^2 = 2\pi \omega |\langle qx \rangle|^2 \frac{E_{rms}^2}{3 \cdot 2} \frac{dN}{dE}$$

$$\alpha = \frac{\pi \omega}{3cn \epsilon_0} |\langle qx \rangle|^2 \frac{dN}{dE}.$$

Now, if the radiation has a blackbody spectrum, we have that the rate of spontaneous emission is

$$\begin{aligned} \frac{1}{\tau_{sp}} &= \int_v \alpha \cdot \frac{8\pi n^2 v^2 dv}{c^2} \frac{1}{e^{hv/k_b T} - 1} \\ &= \int_v \frac{\pi \omega}{3cn \epsilon_0} |\langle qx \rangle|^2 \frac{dN}{dE} \cdot \frac{8\pi n^2 v^2 dv}{c^2} \frac{1}{e^{hv/k_b T} - 1}. \end{aligned}$$

For a two-level system we have that  $dN = \delta(E - E_0)dE = \delta(v - v_0)dv$  and the integral collapses to

$$\frac{1}{\tau_{sp}} = \frac{2|\langle qx \rangle|^2}{3\epsilon_0} \cdot \frac{n(4\pi^2 v^2)\omega}{c^3} \frac{dv}{dE} \frac{1}{e^{hv/k_b T} - 1},$$

where now  $v = v_0$ . Noting that  $dE/dv = h$ , and assuming that  $hv \gg k_b T$ , the expression simplifies to

$$\frac{1}{\tau_{sp}} \approx \frac{2}{3} |\langle qx \rangle|^2 \cdot \frac{\omega^3 n}{c^3 \epsilon_0 h} e^{-hv/k_b T} ,$$

but  $e^{-hv/k_b T} = N_2/N_1$ , which is the ratio of excited two-level systems to ground state two-level systems in case an ensemble of them is at hand. Thus the spontaneous emission rate per unit excited system is

$$\frac{1}{\tau_{sp}} \approx \frac{4}{3} |\langle qx \rangle|^2 \frac{\omega^3 n}{4\pi \epsilon_0 \hbar c^3} .$$

## Method II: Dipole Fluctuations & Zero-Point Fluctuations

Recall the electric potential from a charge distribution  $\rho(x)$  is

$$\phi(x) = \int \frac{\rho(x') d^3 x'}{4\pi \epsilon_0 |x - x'|} .$$

Similarly, the vector potential from a current distribution  $\mathbf{J}(x)$  is

$$\mathbf{A}(x) = \int \frac{\mu_0 \mathbf{J}(x') d^3 x'}{4\pi |x - x'|} .$$

Now, for a single moving electron

$$\int \mathbf{J} d^3 x' = \int \rho \mathbf{v} d^3 x' = \int (\rho d^3 x') \mathbf{v} = q \mathbf{v} ,$$

and it follows that the vector potential and electric field generated by such an electron are given by

$$\mathbf{A}(r) = \frac{\mu_0 q \mathbf{v}}{4\pi r} , \quad \mathbf{E}(r) = -\frac{\partial \mathbf{A}(r)}{\partial t} = \frac{\mu_0 q \dot{\mathbf{v}}}{4\pi r} .$$

The radiated power is given by the product of the group velocity  $c/n$ , the energy density  $n^2 \epsilon_0 E_{rms}^2$ , and a term  $\sin^2 \theta$  which describes the angular projection of power for a dipole radiator:

$$Power\ Radiated = \frac{c}{n} \cdot \epsilon_0 n^2 E_{rms}^2 \cdot \sin^2 \theta = c \epsilon_0 n \cdot \left( \frac{\mu_0 q \dot{\mathbf{v}}}{4\pi r} \right)^2 \cdot \sin^2 \theta \quad (W/m^2) .$$

Integrating over a sphere of radius  $r$  we have

$$Power\ Radiated = \frac{2}{3} \cdot \frac{n|q\ddot{x}|^2}{4\pi\epsilon_0 c^3} = \frac{2}{3} \cdot \frac{n\omega^4 |\langle q\mathbf{x} \rangle|^2}{4\pi\epsilon_0 c^3}$$

$$Photon\ Emission\ Rate = \frac{Power\ Radiated}{\hbar\omega} = \frac{2}{3} \cdot \frac{n\omega^3 |\langle q\mathbf{x} \rangle|^2}{4\pi\epsilon_0 c^3 \hbar} ,$$

which is half the standard free space spontaneous emission rate we obtained from detailed balancing and second quantization. Since any energy level is subject to zero-point fluctuations it acts as a dipole and thus radiates. This also applies to the ground state since

$$\langle i|\mathbf{x}^2|i\rangle = \sum_j \langle i|\mathbf{x}|j\rangle \langle j|\mathbf{x}|i\rangle = \sum_j |\langle i|\mathbf{x}|j\rangle|^2 \neq 0$$

so there must be zero-point fluctuations in the ground state just as there are for an excited state:  $\langle j|\mathbf{x}^2|j\rangle = |\langle i|\mathbf{x}|j\rangle|^2 = \langle i|\mathbf{x}^2|i\rangle$ . This still only gives us half the desired spontaneous emission rate. The rest comes by considering that the zero-point fluctuations are absorbed so that

$$\alpha = \frac{4\pi^2}{cn} \omega \frac{|\langle q\mathbf{x} \rangle|^2}{3} \frac{dN}{dE} .$$

The power flux of zero-point energy is  $c/n$  times the zero-point-field energy density:

$$Power\ Flux = \frac{c}{n} \cdot \frac{\hbar\omega}{2V} \cdot \frac{n^3 \omega^2 V}{\pi^2 \hbar c^3} dE$$

$$\alpha \times Power\ Flux = \frac{4\pi^2}{cn} \omega \frac{|\langle q\mathbf{x} \rangle|^2}{4\pi\epsilon_0 \cdot 3} \cdot \frac{c}{n} \cdot \frac{n^3 \omega^3}{2\pi^2 c^3}$$

$$Energy\ Absorption\ Rate\ per\ Unit\ Volume = \frac{2}{3} \frac{n |\langle q\mathbf{x} \rangle|^2 \omega^4}{4\pi\epsilon_0 c^3}$$

$$Photon\ Absorption\ Rate\ per\ Unit\ Volume = \frac{2}{3} \frac{n |\langle q\mathbf{x} \rangle|^2 \omega^3}{4\pi\epsilon_0 c^3 \hbar}$$

Summing both contributions we obtain the expected rate

$$\frac{1}{\tau_{sp}} = \frac{4}{3} |\langle q\mathbf{x} \rangle|^2 \frac{\omega^3 n}{4\pi\epsilon_0 \hbar c^3} .$$

In other words, the electric dipole moment which vibrates at angular frequency  $\omega_0$ , emits an electromagnetic wave with energy  $\hbar\omega_0$ . Also, the emitted electromagnetic wave reacts on the electric dipole moment. When the atom is in the excited state, the fluctuations in the vacuum field and the electromagnetic wave interact with the same phase, which induces spontaneous

emission. While the atom is in the ground state, the interaction takes place with the antiphase and spontaneous absorption never happens.